ISSN 1069-3513, Izvestiya, Physics of the Solid Earth, 2009, Vol. 45, No. 3, pp. 179–198. © Pleiades Publishing, Ltd., 2009.
Original Russian Text © M.N. Berdichevsky, V.A. Kuznetsov, N.A. Pal'shin, 2009, published in Fizika Zemli, 2009, No. 3, pp. 3–23.

Analysis of Magnetovariational Response Functions

M. N. Berdichevsky[a], V. A. Kuznetsov[b], and N. A. Pal'shin[b]

[a] *Moscow State University, Moscow, 119899 Russia*

[b] *Shirshov Institute of Oceanology, Russian Academy of Sciences, ul. Krasikova 23, Moscow, 117218 Russia*

Received June 30, 2008

Abstract—Advances in magnetovariational sounding are stimulating further development of this area of deep geoelectrics. The paper contains a review of magnetovariational response functions revealing their main properties and proposing new methods of their analysis. The theory of magnetic perturbation ellipses having a higher resolution is set forth and methods of the decomposition of magnetovariational functions are discussed that allow one to reduce 3D magnetovariational interpretation to two or three independent 2D inversions and eliminate the effect of 2D regional structures of the geoelectric background.

PACS numbers: 91.25.Qi

DOI: 10.1134/S106935130903001X

INTRODUCTION

Magnetovariational sounding occupies a particular place among methods using the magnetotelluric field because with a decrease in frequency it is freed from perturbation effects of near-surface heterogeneities and supplies reliable information on deep geoelectric structures (in distinction from magnetotelluric sounding, with its static shift of the apparent resistance, distorting information on deep structures). In the literature, we encounter reports on successful magnetovariational studies performed in Pomerania and Fennoscandia [Varentsov, 2007; Varentsov et al., 2005; Paiunpaa et al., 2002], the Andes [Soyer and Brasse, 2001], the Cascadia subduction zone [Vanyan et al., 2002], and the Tien Shan [Sokolova et al., 2007]. These works are stimulating further development of the magnetovariational method. This paper answers this challenge of the times and is devoted to new methods of analysis of magnetovariational response functions.

MAGNETOVARIATIONAL RESPONSE FUNCTIONS

The magnetovariational response functions are derived from the model of a layered horizontally heterogeneous Earth excited by a plane electromagnetic wave incident vertically onto the flat Earth's surface [Parkinson, 1959; Wiese, 1962; Berdichevsky, 1968; Schmucker, 1970; Berdichevsky and Dmitriev, 2002, 2008; Varentsov, 2007]. We use the right Cartesian coordinate system with horizontal x and y axes and the z axis directed downward. The magnetic field $\mathbf{H}$ is considered as the sum of the normal horizontally polarized field $\mathbf{H}^N$ observed in the absence of horizontal geoelectric heterogeneity and the anomalous field $\mathbf{H}^A$ arising under the action of horizontal geoelectric heterogeneity:

$$\mathbf{H} = \mathbf{H}^N + \mathbf{H}^A, \tag{1}$$

where

$$\mathbf{H} = \begin{bmatrix} H_x \\ H_y \\ H_z \end{bmatrix}, \quad \mathbf{H}^N = \begin{bmatrix} H_x^N \\ H_y^N \end{bmatrix}, \quad \mathbf{H}^A = \begin{bmatrix} H_x^A \\ H_y^A \\ H_z^A \end{bmatrix}. \tag{2}$$

The anomalous magnetic field is defined as the convolution of the Green's magnetic tensor with the excess current propagating in the horizontally heterogeneous Earth.

The following response functions are used in magnetovariational sounding.

The Wiese–Parkinson tipper [W]. This response function goes back to the definitions of Parkinson [Parkinson, 1959] and Wiese [Wiese, 1962]. The Wiese–Parkinson 1×2 matrix $[\mathbf{W}]$ transforms the horizontal magnetic field $\mathbf{H}_\tau(\mathbf{r})$ observed at a field station $O(\mathbf{r})$ into the vertical component $H_z(\mathbf{r}) = H_z^A(\mathbf{r})$ of the anomalous magnetic field $\mathbf{H}^A(\mathbf{r})$ observed at the same station:

$$H_z(\mathbf{r}) = [\mathbf{W}]\mathbf{H}_\tau(\mathbf{r}), \tag{3}$$

where

$$[\mathbf{W}] = [\mathbf{W}(\mathbf{r})] = [W_{zx}(\mathbf{r})W_{zy}(\mathbf{r})],$$
$$\mathbf{H}_\tau(\mathbf{r}) = \begin{bmatrix} H_x(\mathbf{r}) \\ H_y(\mathbf{r}) \end{bmatrix}. \tag{4}$$

The norm of the Wiese–Parkinson matrix

$$\|\mathbf{W}\| = \sqrt{|W_{zx}|^2 + |W_{zy}|^2} \tag{5}$$

is invariant with respect to the rotation of the system (xy) about the z axis. It is minimal over the middle of a

zone of lower or higher resistance and reaches a maximum over the edges of this zone.

The matrix [**W**] is generally represented in the form of the complex vector **W** resolved into components

$$\mathbf{W} = W_{zx}\mathbf{1}_x + W_{zy}\mathbf{1}_y. \quad (6)$$

where $\mathbf{1}_x$ and $\mathbf{1}_y$ are unit vectors.

The real $\mathrm{Re}\,\mathbf{W} = \mathrm{Re}W_{zx}\mathbf{1}_x + \mathrm{Re}W_{zy}\mathbf{1}_y$ and imaginary $\mathrm{Im}\mathbf{W} = \mathrm{Im}W_{zx}\mathbf{1}_x + \mathrm{Im}W_{zy}\mathbf{1}_y$ parts of the vector **W** are referred to as the **Wiese–Parkinson induction arrows**. Real induction arrows possess a noteworthy property: in the understanding of Wiese, they are directed away from the zone of lower resistance toward that of higher resistance.

The horizontal magnetic tensor [M]. This magnetovariational response function was proposed by Berdichevsky as a magnetic analogue of the Doll tensor used in the method of telluric currents [Berdichevsky, 1968]. The tensor [**M**] with a 2×2 matrix transforms the normal magnetic field $\mathbf{H}_\tau^N$, observed at a distant basis (reference) station $B(\mathbf{r}_B)$ into the horizontal magnetic field $\mathbf{H}_\tau$ observed at a field station $O(\mathbf{r})$:

$$\mathbf{H}_\tau(\mathbf{r}) = [\mathbf{M}]\mathbf{H}_\tau^N(\mathbf{r}_B), \quad (7)$$

where

$$\mathbf{H}_\tau(\mathbf{r}) = \begin{bmatrix} H_x(\mathbf{r}) \\ H_y(\mathbf{r}) \end{bmatrix},$$

$$[\mathbf{M}] = [\mathbf{M}(\mathbf{r}|\mathbf{r}_B)] = \begin{bmatrix} M_{xx}(\mathbf{r}|\mathbf{r}_B) & M_{xy}(\mathbf{r}|\mathbf{r}_B) \\ M_{yx}(\mathbf{r}|\mathbf{r}_B) & M_{yy}(\mathbf{r}|\mathbf{r}_B) \end{bmatrix}, \quad (8)$$

$$\mathbf{H}_\tau^N(\mathbf{r}_B) = \begin{bmatrix} H_x^N(\mathbf{r}_B) \\ H_y^N(\mathbf{r}_B) \end{bmatrix}.$$

The norm of the matrix [**M**] is defined as

$$\|\mathbf{M}\| = \sqrt{|M_{xx}|^2 + |M_{xy}|^2 + |M_{yx}|^2 + |M_{yy}|^2}. \quad (9)$$

The norm [$\|\mathbf{M}\|$] is invariant with respect to the rotation of the system (xy) about the z axis. In the case of the horizontally homogeneous Earth, we have $\|\mathbf{M}\| = \sqrt{2}$. The zones with $\|\mathbf{M}\| > \sqrt{2}$ correlate with lower resistance structures, and the zones with $\|\mathbf{M}\| < \sqrt{2}$ correlate with higher resistance structures.

The magnetic disturbance tensor [S]. Schmucker introduced this tensor in a monograph devoted to the analysis of geomagnetic variations [Schmucker, 1970]. It is often referred to as the ***Schmucker tensor***. The Schmucker tensor with a 3×2 matrix transforms the normal magnetic field $\mathbf{H}_\tau^N$, observed at a distant basis (reference) station $B(\mathbf{r}_B)$ into the anomalous magnetic field $\mathbf{H}^A$ observed at a field station $O(\mathbf{r})$:

$$\mathbf{H}^A(\mathbf{r}) = [\mathbf{S}]\mathbf{H}_\tau^N(\mathbf{r}_B), \quad (10)$$

where

$$\mathbf{H}^A(\mathbf{r}) = \begin{bmatrix} H_x^A(\mathbf{r}) \\ H_y^A(\mathbf{r}) \\ H_z^A(\mathbf{r}) \end{bmatrix},$$

$$[\mathbf{S}] = [\mathbf{S}(\mathbf{r}|\mathbf{r}_B)] = \begin{bmatrix} S_{xx}(\mathbf{r}|\mathbf{r}_B) & S_{xy}(\mathbf{r}|\mathbf{r}_B) \\ S_{yx}(\mathbf{r}|\mathbf{r}_B) & S_{yy}(\mathbf{r}|\mathbf{r}_B) \\ S_{zx}(\mathbf{r}|\mathbf{r}_B) & S_{zy}(\mathbf{r}|\mathbf{r}_B) \end{bmatrix}, \quad (11)$$

$$\mathbf{H}_\tau^N(\mathbf{r}_B) = \begin{bmatrix} H_x^N(\mathbf{r}_B) \\ H_y^N(\mathbf{r}_B) \end{bmatrix}.$$

The matrix of the Schmucker tensor can be divided into two matrices: a 2×2 matrix forming the Schmucker horizontal tensor [$\mathbf{S}_\tau$] and a 1×2 matrix forming the *Schmucker tipper* [$\mathbf{S}_z$].

The Schmucker horizontal tensor [$\mathbf{S}_\tau$] transforms the normal magnetic field $\mathbf{H}_\tau^N$, observed at the basis (reference) station $B(\mathbf{r}_B)$ into the anomalous magnetic field $\mathbf{H}_\tau^A$, observed at the field station $O(\mathbf{r})$:

$$\mathbf{H}_\tau^A(\mathbf{r}) = [\mathbf{S}_\tau]\mathbf{H}_\tau^N(\mathbf{r}_B), \quad (12)$$

where

$$\mathbf{H}_\tau^A(\mathbf{r}) = \begin{bmatrix} H_x^A(\mathbf{r}) \\ H_y^A(\mathbf{r}) \end{bmatrix},$$

$$[\mathbf{S}_\tau] = [\mathbf{S}_\tau(\mathbf{r}|\mathbf{r}_B)] = \begin{bmatrix} S_{xx}(\mathbf{r}|\mathbf{r}_B) & S_{xy}(\mathbf{r}|\mathbf{r}_B) \\ S_{yx}(\mathbf{r}|\mathbf{r}_B) & S_{yy}(\mathbf{r}|\mathbf{r}_B) \end{bmatrix}, \quad (13)$$

$$\mathbf{H}_\tau^N(\mathbf{r}_B) = \begin{bmatrix} H_x^N(\mathbf{r}_B) \\ H_y^N(\mathbf{r}_B) \end{bmatrix}.$$

Schmucker defined the tensor [$\mathbf{S}_\tau$] by the two ***horizontal magnetic disturbance vectors***

$$\mathbf{p} = S_{xx}\mathbf{1}_x + S_{yx}\mathbf{1}_y, \quad \mathbf{q} = S_{xy}\mathbf{1}_x + S_{yy}\mathbf{1}_y, \quad (14)$$

which are images of the normal unit fields $\mathbf{H}^{N(x)} = \mathbf{1}_x$ and $\mathbf{H}^{N(y)} = \mathbf{1}_y$ linearly polarized along, respectively, the x and y axes. The real and imaginary vectors

$$\begin{aligned} \mathrm{Re}\ \mathbf{p} &= \mathrm{Re}\ S_{xx}\mathbf{1}_x + \mathrm{Re}\ S_{yx}\mathbf{1}_y \\ \mathrm{Re}\ \mathbf{q} &= \mathrm{Re}\ S_{xy}\mathbf{1}_x + \mathrm{Re}\ S_{yy}\mathbf{1}_y \\ \mathrm{Im}\ \mathbf{p} &= \mathrm{Im}\ S_{xx}\mathbf{1}_x + \mathrm{Im}\ S_{yx}\mathbf{1}_y \\ \mathrm{Im}\ \mathbf{q} &= \mathrm{Im}\ S_{xy}\mathbf{1}_x + \mathrm{Im}\ S_{yy}\mathbf{1}_y \end{aligned} \tag{15}$$

form ***magnetic disturbance arrows***. These vectors turned by $\pi/2$ yield an illustrative qualitative pattern of the spread of active and reactive anomalous (excess) currents.

The invariant norm of the Schmucker tensor is determined as

$$\|\mathbf{S}_\tau\| = \sqrt{|S_{xx}|^2 + |S_{xy}|^2 + |S_{yx}|^2 + |S_{yy}|^2}. \tag{16}$$

The Schmucker tipper $[\mathbf{S}_z]$ transforms the normal magnetic field $\mathbf{H}^N_\tau$, observed at the distant basis (reference) station $B(\mathbf{r}_B)$ into the vertical component $H_z(\mathbf{r}) = \mathbf{H}^A_z(\mathbf{r})$ of the anomalous magnetic field $\mathbf{H}^A$ observed at the field station $O(\mathbf{r})$:

$$\mathbf{H}_z(\mathbf{r}) = [\mathbf{S}_z]\mathbf{H}^N_\tau(\mathbf{r}_B), \tag{17}$$

where

$$[\mathbf{S}_z] = [\mathbf{S}_z(\mathbf{r}|\mathbf{r}_B)] = \left[S_{zx}(\mathbf{r}|\mathbf{r}_B)\ S_{zy}(\mathbf{r}|\mathbf{r}_B)\right],$$
$$\mathbf{H}^N_\tau(\mathbf{r}_B) = \begin{bmatrix} H^N_x(\mathbf{r}_B) \\ H^N_y(\mathbf{r}_B) \end{bmatrix}. \tag{18}$$

The invariant norm of the Schmucker tipper is defined as

$$\|\mathbf{S}_z\| = \sqrt{|S_{zx}|^2 + |S_{zy}|^2}. \tag{19}$$

By analogy with (6), the matrix $[\mathbf{S}_z]$ is represented in the form of a complex vector

$$\mathbf{S}_z = S_{zx}\mathbf{1}_x + S_{zy}\mathbf{1}_y. \tag{20}$$

The real $\mathrm{Re}\mathbf{S}_z = \mathrm{Re}S_{zx}\mathbf{1}_x + \mathrm{Re}S_{zy}\mathbf{1}_y$ and imaginary $\mathrm{Im}\mathbf{S}_z = \mathrm{Im}S_{zx}\mathbf{1}_x + \mathrm{Im}S_{zy}\mathbf{1}_y$ parts of the vector $\mathbf{S}_z$ form the ***Schmucker induction arrows***. In the Wiese agreement, the real Schmucker induction arrows are directed away from the zone of lower resistance toward that of higher resistance.

The tensors $[\mathbf{S}_\tau]$ and $[\mathbf{M}]$ and the tippers $[\mathbf{S}_z]$and $[\mathbf{W}]$ are connected through the simple relations

$$\begin{aligned} [\mathbf{M}] &= [\mathbf{S}_\tau] + [\mathbf{I}] \\ [\mathbf{W}] &= [\mathbf{S}_z][\mathbf{M}]^{-1}, \end{aligned} \tag{21}$$

where

$$[\mathbf{I}] = \begin{bmatrix} 1 & 0 \\ 0 & 1 \end{bmatrix}.$$

For a 2D model striking along the x axis, we have

$$[\mathbf{W}] = \begin{bmatrix} 0 & W_{zy} \end{bmatrix}, \quad [\mathbf{M}] = \begin{bmatrix} 1 & 0 \\ 0 & M_{yy} \end{bmatrix},$$
$$[\mathbf{S}_z] = \begin{bmatrix} 0 & S_{zy} \end{bmatrix}, \quad [\mathbf{S}_\tau] = \begin{bmatrix} 0 & 0 \\ 0 & S_{yy} \end{bmatrix}. \tag{22}$$

Here real and imaginary induction arrows are perpendicular to the model strike.

MAGNETIC DISTURBANCE ELLIPSES

The magnetic disturbance vectors (arrows) Re$\mathbf{p}$, Im$\mathbf{p}$ and Re$\mathbf{q}$, Im$\mathbf{q}$ defined according to (14) and (15) characterize anomalies of the horizontal components of the anomalous magnetic field corresponding to the normal unit field polarized linearly along the x and y axes. Evidently, the value and orientation of the disturbance vectors depends on an arbitrary choice of a reference system. This indeterminacy can be easily eliminated by the reconstruction of the magnetic disturbance vectors and their incorporation into ***magnetic disturbance ellipses***, which are an analogue of the Doll telluric ellipses [Berdichevsky, 1968; Fujiwara and Toh, 1996]. The magnetic disturbance ellipses are invariant with respect to the rotation of the system (x, y).

Now we will show how to construct the magnetic disturbance ellipses. We introduce the following notation:

$$\begin{aligned} H^N_x = X, \quad H^N_y = Y, \quad H^A_x = U, \quad H^A_y = V, \\ a = \mathrm{Re}S_{xx}, \quad b = \mathrm{Re}S_{xy}, \\ c = \mathrm{Re}S_{yx}, \quad d = \mathrm{Re}S_{yy}, \end{aligned} \tag{23}$$

where the components X and Y of the normal field at the basis point and the components U and V of the anomalous field at the observation point are real quantities. In this notation, the real part of the horizontal Schmucker tensor transforms the plane (XY) into the plane (UV):

$$\begin{aligned} U &= aX + bY, \\ V &= cX + dY. \end{aligned} \tag{24}$$

Consequently, the unit circle $X^2 + Y^2 = 1$ lying in the plane (XY) transforms into the real magnetic disturbance ellipse

$$\begin{aligned} (c^2 + d^2)U^2 - 2(bd + ac)UV \\ + (a^2 + b^2)V^2 = (ad - bc)^2, \end{aligned} \tag{25}$$

lying in the plane (UV). This transformation is exemplified in Fig. 1. Here the vectors of real magnetic distur-

bance Re**p** and Re**q** are the conjugated radii of the ellipse and are the transforms of the conjugated radii $\mathbf{1}_x$ and $\mathbf{1}_y$ of the unit circle. We see that the disturbance ellipse determining the dependence of the horizontal magnetic anomalies on the direction reflects the "magnetic anisotropy" significantly better than the disturbance vectors. The major and minor axes of the ellipse give an idea of the maximum and minimum strength of the horizontal magnetic anomalies. Moreover, the major axis of the ellipse turned by an angle of 90° characterizes the direction and intensity of the maximum anomalous current.

The canonical equation of the real ellipse of a magnetic disturbance has the form

$$\frac{(U')^2}{A^2} + \frac{(V')^2}{B^2} = 1, \tag{26}$$

where

$$A = \sqrt{\frac{a^2+b^2+c^2+d^2}{2} + \sqrt{\frac{(a^2+b^2+c^2+d^2)^2}{4} - (ad-bc)^2}},$$
$$B = \sqrt{\frac{a^2+b^2+c^2+d^2}{2} - \sqrt{\frac{(a^2+b^2+c^2+d^2)^2}{4} - (ad-bc)^2}}, \tag{27}$$

are the major and minor semiaxes of the ellipse. The slope of the major axis of the ellipse is determined as

$$\tan\alpha = \frac{c^2+d^2-a^2-b^2-2(ac+bd)+\sqrt{(a^2+b^2+c^2+d^2)^2-4(ad-bc)^2}}{c^2+d^2-a^2-b^2+2(ac+bd)-\sqrt{(a^2+b^2+c^2+d^2)^2-4(ad-bc)^2}}. \tag{28}$$

We have $a = b = c = 0$ for a 2D model striking along the x axis, and, consequently, $A = d = \mathrm{Re}S_{yy}$, $B = 0$, and $\alpha = \pi/2$. Here the real magnetic disturbance ellipse degenerates into a segment of a straight line oriented along the y axis, i.e., normally to the model strike.

The imaginary magnetic disturbance ellipse related to the vectors Im**p** and Im**q** is constructed analogously. To do this, it is sufficient to substitute

$$a = \mathrm{Im}S_{xx}, \quad b = \mathrm{Im}S_{xy}, \quad c = \mathrm{Im}S_{yx}, \quad d = \mathrm{Im}S_{yy}, \tag{29}$$

into (27) and (28).

As an example we consider the magnetic disturbance ellipses obtained for the model of a 3D graben whose length is three times larger than its width. This model is shown in Fig. 2. Here the transverse conductance of sediments varies from 5 S outside the graben to 100 S within it. Maps of the major and minor axes of real and imaginary ellipses over the fourth quadrant of the graben and in its vicinity are shown in Fig. 3. Note two remarkable features of these maps: (1) the major axes of the ellipses "flow around" the lateral flanks of the graben and (2) they are directed perpendicularly to the graben strike in its central part. The maps showing the major axes of the ellipses turned by 90°, which characterize the direction and intensity of the maximum anomalous current (Fig. 4), clarify the physical meaning of these features. The effect of the channeling of currents is clearly seen here: active and reactive anomalous currents flow into the graben and concentrate along its strike.

PROPERTIES OF 2D MAGNETOVARIATIONAL RESPONSE FUNCTIONS

Figure 5 shows layered geoelectric models of the tectonosphere including a three-layer sedimentary cover $(\rho_1', h_1'; \rho_1'', h_1''; \rho_1''', h_1''')$,, two-layer crust $(\rho_2', h_2'; \rho_2'', h_2'')$, and two-layer mantle $(\rho_3', h_3'; \rho_3'', h_3'')$. These models contain infinitely long 2D structures represented by prisms P_1, P_2, and P_3 of various strike. The angles of strike α', α'', and α''' are counted clockwise from the x axis. Prism P_1 of width w' and resistivity ρ' is included in the high-resistance mantle (layer ρ_3'). It imitates a low-resistance asthenolith. Prism P_2 of width w'' and resistivity ρ'' is included in the high-resistance consolidated Earth's crust (layer ρ_2'). It imitates a low-resistance graphitization zone. Prism P_3 of width w''' and resistivity ρ''' is included in the low-resistance sedimentary cover (layer ρ_1'). It imitates a high-resistance horst. Thus, we have 2D models $\{P_1\}$, $\{P_2\}$, and $\{P_3\}$ and their 3D superpositions $\{P_1P_2\}$ and $\{P_1P_2P_3\}$.

Figure 6 plots the pseudotopography of the norms of the tippers and horizontal magnetic tensors $\|\mathbf{W}\|$, $\|\mathbf{S}_z\|$ and $\|\mathbf{M}\|$, $\|\mathbf{S}_\tau\|$ calculated for the model $\{P_1P_2P_3\}$ from formulas (5), (19) and (9), (16). This 3D many-tier model demonstrates a number of important properties of the magnetovariational response functions.

Considering the pseudotopography of the norms $\|\mathbf{W}\|$, $\|\mathbf{S}_z\|$ and $\|\mathbf{M}\|$, $\|\mathbf{S}_\tau\|$, we identify periods $T = 0.1, 20,$

100, and 1000 s at which individual structures dominate. Thus, the pseudoterrains $\|\mathbf{W}\|$, $\|\mathbf{S}_z\|$ and $\|\mathbf{M}\|$, $\|\mathbf{S}_\tau\|$ reflect a "pure" 2D effect of the horst P_3 at $T = 0.1$ s. This near-surface effect attenuates with a frequency decrease, giving way to deep effects. The 2D effect of the graphitization zone P_2 becomes distinct at periods T = 20–100 s, with the effect of the horst vanishing and that of the asthenolith being more or less weak. Finally, we have a powerful 2D effect of the asthenolith and a vanishing effect of the graphitization zone at the period T = 10000. Each structure has its place in the period scale. One gets the impression that the "structure superposition principle" acts here: because galvanic and inductive coupling are weak, the additive effect of the structures is approximately equal to the sum of the effects of each structure.

The following properties of the magnetovariational response function are seen on the pseudotopography maps.

1. The strike of the pseudotopographies $\|\mathbf{W}\|$, $\|\mathbf{S}_z\|$ and $\|\mathbf{M}\|$, $\|\mathbf{S}_\tau\|$ nearly coincides with the strike of the anomaly-forming structures at periods of the domination of some 2D structure or other.

2. Returning to periods T = 20–100 s, we see that, at T = 20 s, the pseudotopographies $\|\mathbf{M}\|$, $\|\mathbf{S}_\tau\|$ of horizontal magnetic tensors clearly reflect the crustal graphitization zone P_2. At the same time, indications of the asthenolith P_1 are seen on the pseudotopographies $\|\mathbf{W}\|$, $\|\mathbf{S}_z\|$ of the tippers together with the dominating graphitization zone P_2. Discernible indications of the asthenolith arise on the psedotopographies $\|\mathbf{M}\|$, $\|\mathbf{S}_\tau\|$ at T = 100 s and these indications become quite significant on the pseudotopographies $\|\mathbf{W}\|$, $\|\mathbf{S}_z\|$. Evidently, the tippers have a higher sensitivity to deep structures.

3. At low frequencies (T = 100–10000 s), the shape of the pseudotopographies $\|\mathbf{M}\|$, $\|\mathbf{S}_\tau\|$ of the horizontal magnetic tensors is smooth and is typical of diffused fields; they consist of a single range rising over the middle of the structure, with its slopes extending far outside the structure. At the same time, the pseudotopographies $\|\mathbf{W}\|$, $\|\mathbf{S}_z\|$ of the tippers consist of two parallel ranges rising over the structure edges. A deep valley lying over the middle of the structure separates these ranges. We can say that the tippers yield the "vertical projection" of the structure edges on the Earth's surface. The structure width is determined here with a sufficient accuracy. Evidently, the tippers, reflecting the asymmetry of excess currents, resolve horizontal variations in the deep conduction considerably better than the horizontal magnetic tensors.

4. The pseudotopographies $\|\mathbf{W}\|$, $\|\mathbf{S}_z\|$ of the Wiese–Parkinson and Schmucker tippers are close to each other. This is accounted for by the fact that the horizontal components of the anomalous magnetic field in the study model are significantly smaller than the normal magnetic field.

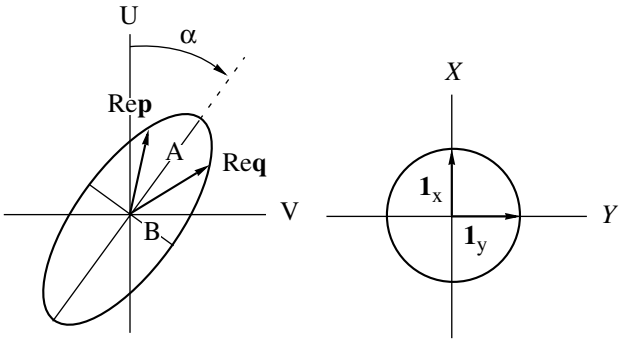

Fig. 1. The magnetic disturbance vectors Re**p** and Im**p** are the conjugated radii of the magnetic disturbance ellipse.

DECOMPOSITION OF THE MAGNETOVARIATIONAL RESPONSE FUNCTIONS

We suppose in the preceding part of the paper that the structure superposition principle acts in the many-tier model including three 2D structures (the mantle asthenolith P_1, crustal graphitization zone P_2, and horst P_3), i.e., the additive magnetovariational effect of all the three structures is approximately equal to the sum of the partial effects of each structure. Now we will evaluate the accuracy of such an approximation for weak conductive and inductive coupling between the structures. We will consider three problems of decomposition of

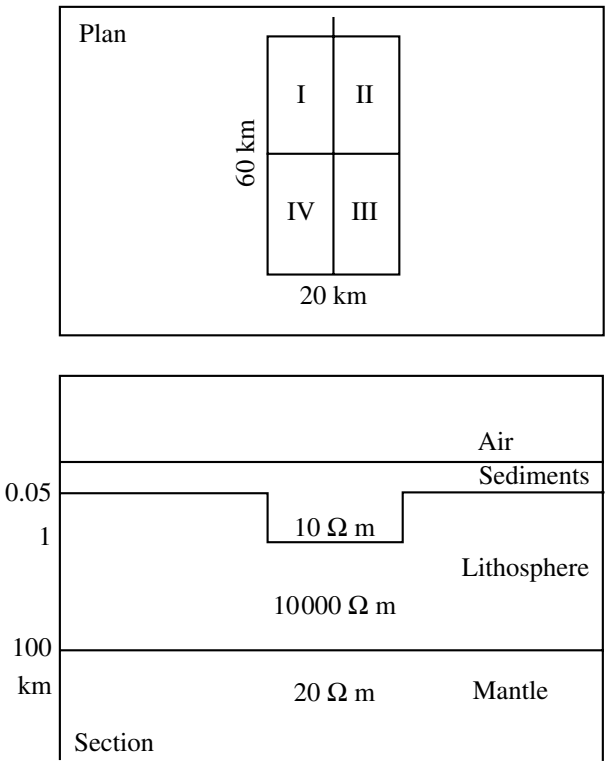

Fig. 2. Model of a 3D graben.

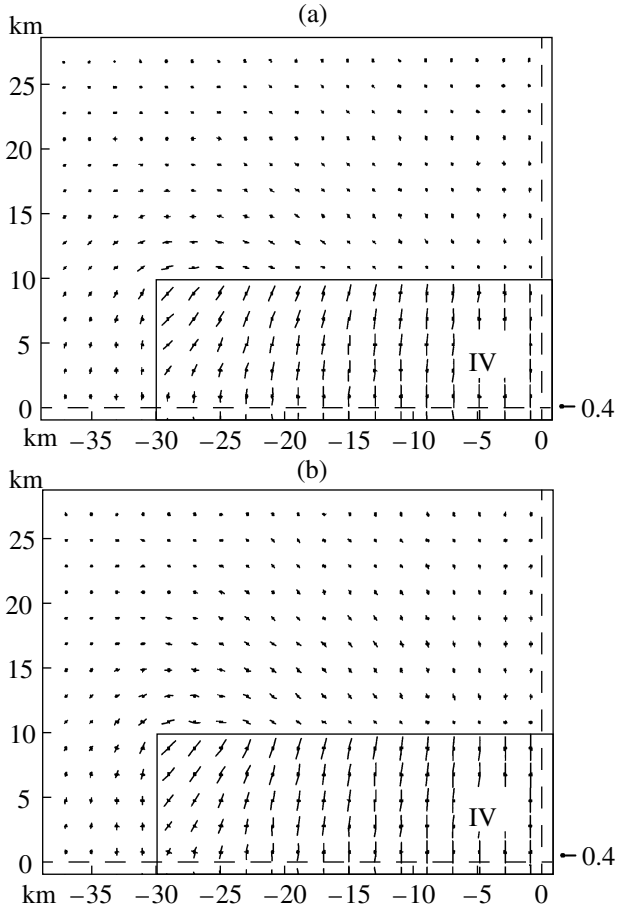

Fig. 3. Maps showing the major and minor axes of the magnetic disturbance ellipses over quadrant IV of the graben and its neighborhood, T = 10 s: (a) real ellipse; (b) imaginary ellipse.

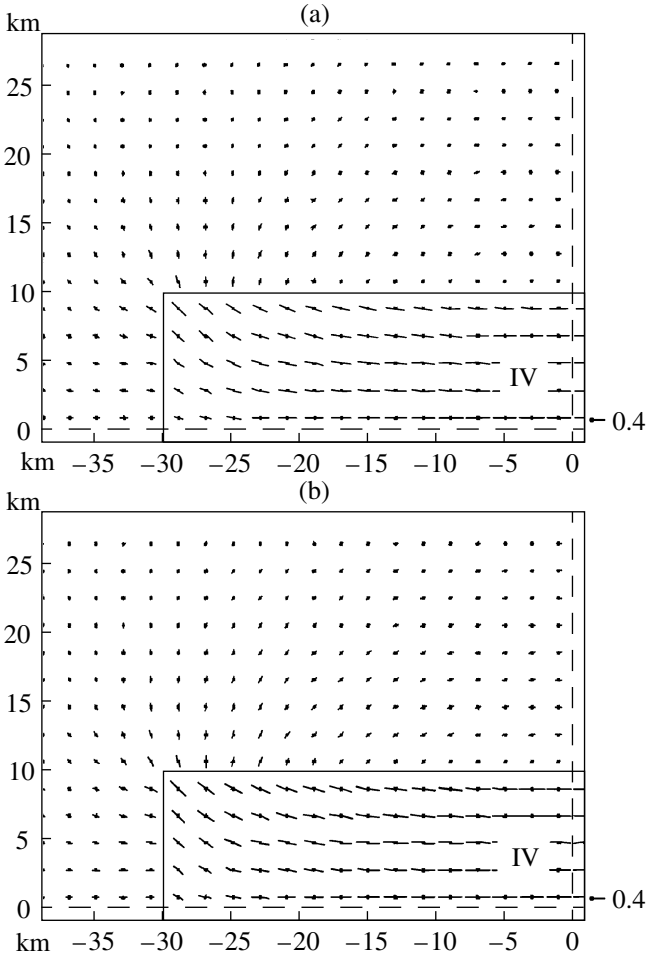

Fig. 4. Maps showing the major axes of the magnetic disturbance ellipses turned by 90°, which characterize the direction and intensity of the maximum anomalous current in the graben and its neighborhood, T = 10 s: (a) real ellipse; (b) imaginary ellipse.

the magnetovariational response functions provided that the interaction between structures is sufficiently weak and differences in their strikes are sufficiently great.

The first problem is to decompose the magnetovariational response functions in the model $\{P_1P_2P_3\}$ containing three 2D structures P_1, P_2, and P_3. These structures shown in Fig. 5 are identified with the asthenolith, graphitization zone, and horst. This problem is formulated as follows. The matrix $[\mathbf{S}_\tau]$ of the Schmucker horizontal tensor determining the additive effect of the 2D structures P_1, P_2, and P_3 is obtained from synchronous magnetovariational observations. The matrix $[\mathbf{S}_\tau]$ is taken as initial. It is necessary to obtain (a) the partial matrix $[\mathbf{S}'_\tau]$, determining the effect of the structure P_1 in the absence of the structures P_2 and P_3, (b) the partial matrix $[\mathbf{S}''_\tau]$, determining the effect of the structure P_2 in the absence of the structures P_1 and P_3, and (c) the partial matrix $[\mathbf{S}'''_\tau]$, determining the effect of the structure P_3 in the absence of the structures P_1 and P_2. The problem is solved in several stages.

At the first stage, the pseudotopographies of $\|\mathbf{S}_\tau\|$ are constructed and the angles of strike α', α'', and α''' of, respectively, the structures P_1, P_2, and P_3 counted from the x axis of the measuring coordinate system (xy) are determined. Then partial coordinate systems ($x'y'$, $x''y''$), and ($x'''y'''$) are introduced with the x', x'', and x''' axes directed along the strike of the respective structures. According to (22), we have in these coordinates

$$[\mathbf{S}'_\tau] = \begin{bmatrix} 0 & 0 \\ 0 & \mathbf{S}'_\tau \end{bmatrix}, \quad [\mathbf{S}''_\tau] = \begin{bmatrix} 0 & 0 \\ 0 & \mathbf{S}''_\tau \end{bmatrix}, \quad [\mathbf{S}'''_\tau] = \begin{bmatrix} 0 & 0 \\ 0 & \mathbf{S}'''_\tau \end{bmatrix}. \tag{30}$$

At the second stage, the measuring coordinate system (xy) is turned by an angle of α' and brought into coincidence with the partial coordinate system ($x'y'$).

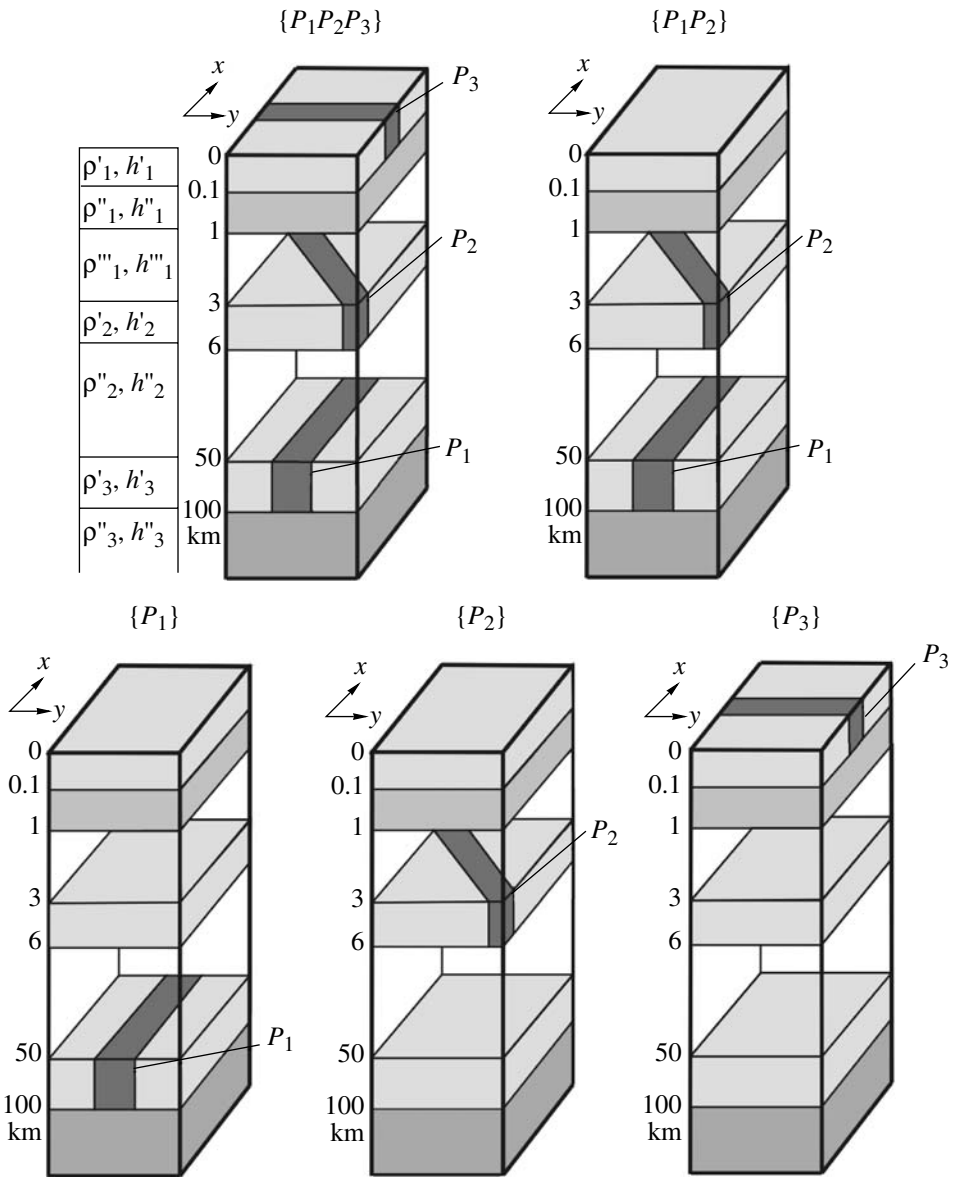

Fig. 5. Geoelectric models $\{P_1\}$, $\{P_2\}$, $\{P_3\}$, $\{P_1P_2\}$, and $\{P_1P_2P_3\}$ of the tectonosphere including single 2D structures P_1, P_2, P_3 of various strike and their 3D superpositions $P_1 + P_2$ and $P_1 + P_2 + P_3$. Parameters of the normal section: sedimentary cover $\rho'_1 = 10\ \Omega$ m, $h'_1 = 0.1$ km; $\rho''_1 = 1000\ \Omega$ m, $h''_1 = 0.9$ km; $\rho'''_1 = 100\ \Omega$ m, $h'''_1 = 2$ km; Earth's crust: $\rho'_2 = 1000\ \Omega$ m; $h'_2 = 3$ km; $\rho''_2 = 1000\ \Omega$ m, $h''_2 = 44$ km; mantle: $\rho'_3 = 1000\ \Omega$ m, $h'_3 = 50$ km; $\rho''_3 = 20\ \Omega$ m, $h''_3 = \infty$. Structure parameters: $P_1 - \alpha' = 0$, $w' = 300$ km, $\rho' = 5\ \Omega$ m; $P_2 - \alpha'' = 135°$, $w'' = 100$ km, $\rho'' = 6\ \Omega$ m; $P_3 - \alpha''' = 90°$, $w''' = 32$ km, $\rho'' = 1000\ \Omega$ m.

The angles of strike of the structures P_1, P_2, and P_3 are defined in the turned coordinate system (xy) as

$$\beta' = \alpha' - \alpha' = 0, \quad \beta'' = \alpha'' - \alpha', \quad \beta''' = \alpha''' - \alpha', \tag{31}$$

and matrices $[\boldsymbol{S}_\tau]$ and $[\mathbf{S}'_\tau]$, $[\mathbf{S}''_\tau]$, $[\mathbf{S}'''_\tau]$ take the form

$$[\mathbf{S}_\tau] = \begin{bmatrix} S_{xx} & S_{xy} \\ S_{yx} & S_{yy} \end{bmatrix}, \quad [\mathbf{S}'_\tau(\beta')] = \begin{bmatrix} 0 & 0 \\ 0 & S'_\tau \end{bmatrix},$$

$$[\mathbf{S}''_\tau(\beta'')] = S''_\tau \begin{bmatrix} \sin^2\beta'' & -\sin\beta''\cos\beta'' \\ -\sin\beta''\cos\beta'' & \cos^2\beta'' \end{bmatrix}, \tag{32}$$

$$[\mathbf{S}'''_\tau(\beta''')] = S'''_\tau \begin{bmatrix} \sin^2\beta''' & -\sin\beta'''\cos\beta''' \\ -\sin\beta'''\cos\beta''' & \cos^2\beta''' \end{bmatrix}.$$

At the final stage, we neglect the interaction between the structures and assume that the additive

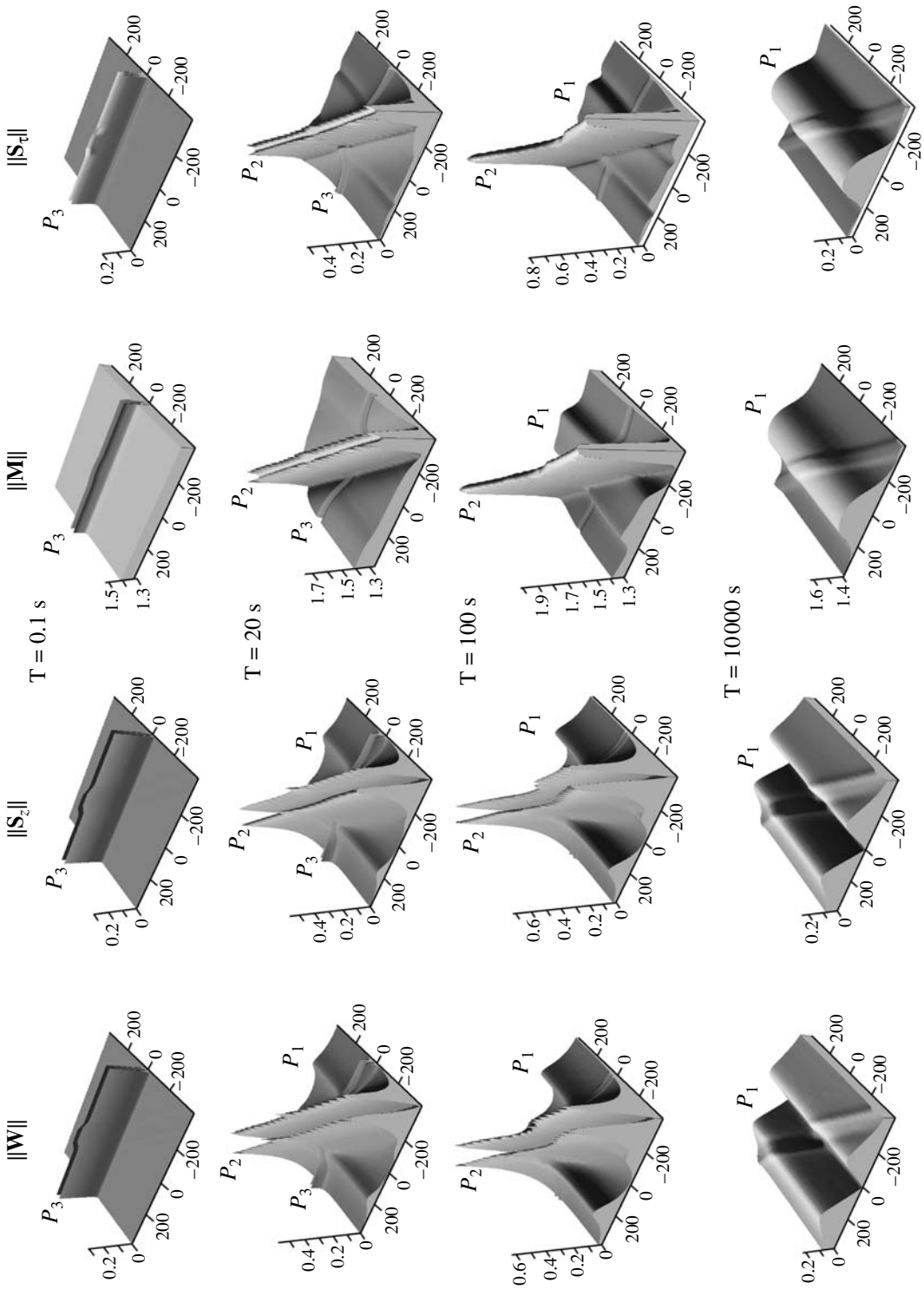

Fig. 6. The pseudotopographies of the norms $\|\mathbf{W}\|$, $\|\mathbf{S}_z\|$ and $\|\mathbf{M}\|$, $\|\mathbf{S}_\tau\|$ of the tipper and horizontal magnetic tensor matrices in the model $\{P_1P_2P_3\}$ shown in Fig. 5.

magnetic anomaly $\mathbf{H}_\tau^A$ is equal to the sum of the partial magnetic anomalies $(\mathbf{H}_\tau^A)'$, $(\mathbf{H}_\tau^A)''$, and $(\mathbf{H}_\tau^A)'''$. In this approximation,

$$\begin{aligned}\mathbf{H}_\tau^A &= (\mathbf{H}_\tau^A)' + (\mathbf{H}_\tau^A)'' + (\mathbf{H}_\tau^A)''' \\ &= [\mathbf{S}_\tau'(\beta')]\mathbf{H}^N + [\mathbf{S}_\tau''(\beta'')]\mathbf{H}^N + [\mathbf{S}_\tau'''(\beta''')]\mathbf{H}^N \\ &= \{[\mathbf{S}_\tau'(\beta')] + [\mathbf{S}_\tau''(\beta'')] + [\mathbf{S}_\tau'''(\beta''')]\}\mathbf{H}^N = [\tilde{\mathbf{S}}_\tau]\mathbf{H}^N,\end{aligned} \tag{33}$$

where with regard for (32)

$$[\tilde{\mathbf{S}}_\tau] = [\mathbf{S}'_\tau(\beta')] + [\mathbf{S}''_\tau(\beta'')] + [\mathbf{S}'''_\tau(\beta''')]$$
$$= \begin{bmatrix} \sin^2\beta'' S''_\tau + \sin^2\beta''' S'''_\tau & -\sin\beta''\cos\beta'' S''_\tau - \sin\beta'''\cos\beta''' S'''_\tau \\ -\sin\beta''\cos\beta'' S''_\tau - \sin\beta'''\cos\beta''' S'''_\tau & S' + \cos^2\beta'' S''_\tau + \cos^2\beta''' S'''_\tau \end{bmatrix}. \quad (34)$$

Equating the symmetric matrix $[\tilde{\mathbf{S}}_\tau]$ to the initial matrix $[\mathbf{S}_\tau]$, we obtain the overdetermined system of four incompatible equations in three unknowns $\mathbf{S}'_\tau$, $\mathbf{S}''_\tau$, and $\mathbf{S}'''_\tau$:

$$\begin{aligned} S''_\tau \sin^2\beta'' + S'''_\tau \sin^2\beta''' &= S_{xx}, \\ S''_\tau \sin\beta''\cos\beta'' + S'''_\tau \sin\beta'''\cos\beta''' &= -S_{xy}, \\ S''_\tau \sin\beta''\cos\beta'' + S'''_\tau \sin\beta'''\cos\beta''' &= -S_{yx}, \\ S' + S''_\tau \cos^2\beta'' + S'''_\tau \cos^2\beta''' &= S_{yy}. \end{aligned} \quad (35)$$

Applying the principle of least squares, we reduce this system of conditional equations to a system of three normal equations. We have in the matrix form

$$\begin{bmatrix} 1 & k & l \\ k & 1 & m \\ l & m & 1 \end{bmatrix} \begin{bmatrix} \mathbf{S}'_\tau \\ \mathbf{S}''_\tau \\ \mathbf{S}'''_\tau \end{bmatrix} = \begin{bmatrix} A \\ B \\ C \end{bmatrix}, \quad (36)$$

where

$$k = \cos^2\beta'' \quad A = S_{yy}$$
$$l = \cos^2\beta'''$$
$$B = S_{xx}\sin^2\beta'' - (S_{xy} + S_{yx})\sin\beta''\cos\beta'' + S_{yy}\cos^2\beta''$$
$$m = \cos^2(\beta''' - \beta'')$$
$$C = S_{xx}\sin^2\beta''' - (S_{xy} + S_{yx})$$
$$\times \sin\beta'''\cos\beta''' + S_{yy}\cos^2\beta'''.$$

Solving the normal equations, we obtain

$$\begin{aligned} S'_\tau &= \frac{A(m^2-1) + B(k-lm) + C(l-km)}{k^2 + l^2 + m^2 - 2klm - 1}, \\ S''_\tau &= \frac{A(k-lm) + B(l^2-1) + C(m-kl)}{k^2 + l^2 + m^2 - 2klm - 1}, \\ S'''_\tau &= \frac{A(l-km) + B(m-kl) + C(k^2-1)}{k^2 + l^2 + m^2 - 2klm - 1}. \end{aligned} \quad (37)$$

Substituting (37) into (32), we determine the partial matrices $[\mathbf{S}'_\tau]$, $[\mathbf{S}''_\tau]$, and $[\mathbf{S}'''_\tau]$,, the sum $[\tilde{\mathbf{S}}_\tau]$ of which approaches the initial matrix $[\mathbf{S}_\tau]$.

Figure 7 demonstrates the decomposition of the magnetovariational functions in the model $\{P_1P_2P_3\}$ shown in Fig. 5. Here the initial matrix $[\mathbf{S}_\tau]$ is decomposed into three partial matrices $[\mathbf{S}'_\tau]$, $[\mathbf{S}''_\tau]$, , and $[\mathbf{S}'''_\tau]$. We see that in a wide range of periods T (0.1–1000 s) the pseudotopographies $\|\mathbf{S}'_\tau\|$, $\|\mathbf{S}''_\tau\|$, and $\|\mathbf{S}'''_\tau\|$ of the partial matrices $[\mathbf{S}'_\tau]$, $[\mathbf{S}''_\tau]$, and $[\mathbf{S}'''_\tau]$, obtained via the decomposition of the initial matrix $[\mathbf{S}_\tau]$ are close to the pseudotopographies $\|\bar{\mathbf{S}}'_\tau\|$, $\|\bar{\mathbf{S}}''_\tau\|$, and $\|\bar{\mathbf{S}}'''_\tau\|$ of the partial matrices $[\bar{\mathbf{S}}'_\tau]$, $[\bar{\mathbf{S}}''_\tau]$, and $[\bar{\mathbf{S}}'''_\tau]$, obtained for the models $\{P_1\}$, $\{P_2\}$, and $\{P_3\}$ by direct calculations. This evidences the sufficient accuracy of the decomposition. We conclude that the pseudotopography of the norm of each of the partial matrices $[\mathbf{S}'_\tau]$, $[\mathbf{S}''_\tau]$ and $[\mathbf{S}'''_\tau]$ reflects the dominating effect of the corresponding anomaly-forming structure. Thus, the inversion of the 3D matrices $[\mathbf{S}_\tau]$ may be reduced to three independent inversions of the 2D matrices $[\mathbf{S}'_\tau]$, $[\mathbf{S}''_\tau]$, and $[\mathbf{S}'''_\tau]$. .

The second problem is to decompose the magnetovariational response functions in the model $\{P_1P_2\}$ containing two 2D structures P_1 and P_2 imitating the asthenolith and crustal graphitization zone. The second problem is formulated as follows. The matrices $[\mathbf{S}_\tau]$ and $[\mathbf{S}_z]$ of the Schmucker horizontal tensor and Schmucker tipper determining the additive effects of the 2D structures P_1 and P_2 are obtained from synchronous magnetovariational observations. The matrices $[\mathbf{S}_\tau]$ and $[\mathbf{S}_z]$ are considered as initial. It is necessary to obtain (a) the partial matrices $[\mathbf{S}'_\tau]$ and $[\mathbf{S}'_z]$ determining the effect of the structure P_1 in the absence of the structure P_2 and (b) the partial matrices $[\mathbf{S}''_\tau]$ and $[\mathbf{S}''_z]$, determining the effect of the structure P_2 in the absence of the structure P_1. The method of computation in the second problem is the same as in the first problem.

At the first stage, the pseudotopographies $\|\mathbf{S}_\tau\|$ and $\|\mathbf{S}_z\|$ are constructed and the angles of strike α' and α'' of the structures P_1 and P_2 counted from the x axis of the

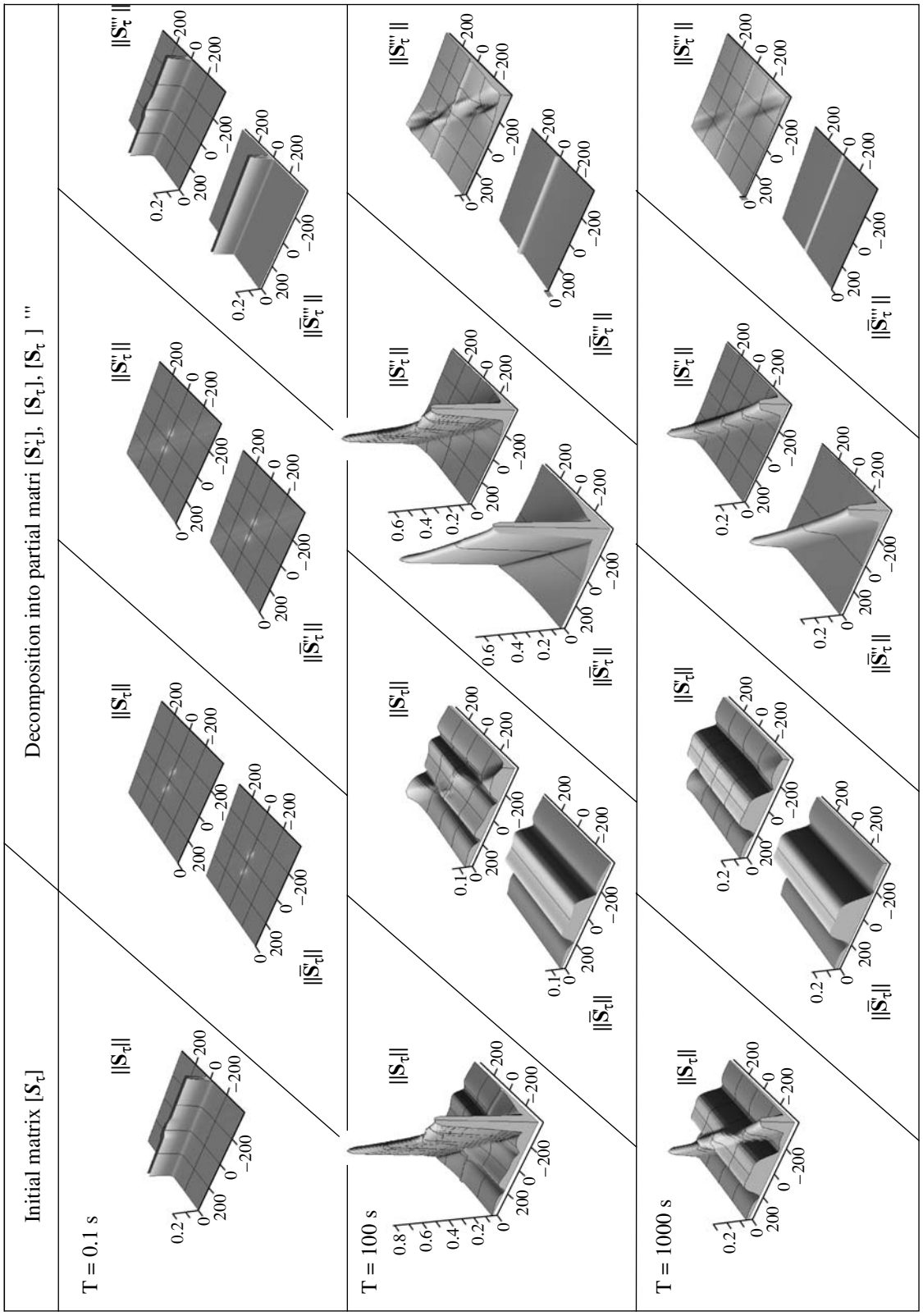

Fig. 7. The decomposition of the initial matrix $[\mathbf{S}_\tau]$ of the Schmucker horizontal magnetic tensor into three partial matrices $[\mathbf{S}'_\tau]$,$[\mathbf{S}''_\tau]$ and $[\mathbf{S}'''_\tau]$ in the model $\{P_1P_2P_3\}$ shown in Fig. 5.

measuring coordinate system (xy) are obtained in favorable frequency intervals. Then we introduce the partial coordinate systems ($x'y'$) and ($x''y''$) with the axes x' and x'' directed along the strike of the respective structures. According to (22), we have in these coordinates

$$[\mathbf{S}'_\tau] = \begin{bmatrix} 0 & 0 \\ 0 & S'_\tau \end{bmatrix}, \quad [\mathbf{S}''_\tau] = \begin{bmatrix} 0 & 0 \\ 0 & S''_\tau \end{bmatrix},$$
$$[\mathbf{S}'_z] = [0\ S'_z], \quad [\mathbf{S}''_z] = [0\ S''_z], \tag{38}$$

At the second stage, we turn the measuring coordinate system (xy) by an angle of α' and bring it into coincidence with the partial coordinate system ($x'y'$). The angles of strike of the structures P_1 and P_2 are defined in the turned coordinate system as

$$\beta' = \alpha' - \alpha' = 0 \quad \beta'' = \alpha'' - \alpha', \tag{39}$$

and the matrices $[\mathbf{S}_\tau]$, $[\mathbf{S}'_\tau]$, and $[\mathbf{S}''_\tau]$ and $[\mathbf{S}_z]$, $[\mathbf{S}'_z]$, and $[\mathbf{S}''_z]$ take the form

$$[\mathbf{S}_\tau] = \begin{bmatrix} S_{xx} & S_{xy} \\ S_{yx} & S_{yy} \end{bmatrix},$$
$$[\mathbf{S}'_\tau] = \begin{bmatrix} 0 & 0 \\ 0 & S'_\tau \end{bmatrix},$$
$$[\mathbf{S}''_\tau] = S''_\tau \begin{bmatrix} \sin^2\beta'' & -\sin\beta''\cos\beta'' \\ -\sin\beta''\cos\beta'' & \cos^2\beta'' \end{bmatrix}, \tag{40}$$
$$[\mathbf{S}_z] = \begin{bmatrix} S_{zx} & S_{zy} \end{bmatrix}, \quad [\mathbf{S}'_z] = \begin{bmatrix} 0 & S'_z \end{bmatrix},$$
$$[\mathbf{S}''_z] = S''_z \begin{bmatrix} -\sin\beta'' & \cos\beta'' \end{bmatrix}.$$

At the final stage, we neglect the interaction between the structures and assume that the additive magnetic anomalies $\mathbf{H}^A_\tau$ and $H_z = H^A_z$ are equal to the sums of the partial magnetic anomalies $((\mathbf{H}^A_\tau)', (\mathbf{H}^A_\tau)''$ and H'_z, H''_z. In this approximation,

$$\mathbf{H}^A_\tau = (\mathbf{H}^A_\tau)' + (\mathbf{H}^A_\tau)'' = [\mathbf{S}'_\tau]\mathbf{H}^N + [\mathbf{S}''_\tau]\mathbf{H}^N$$
$$= \{[\mathbf{S}'_\tau] + [\mathbf{S}''_\tau]\}\mathbf{H}^N = [\tilde{\mathbf{S}}_\tau]\mathbf{H}^N \tag{41}$$

and

$$H_z = H'_z + H''_z = [\mathbf{S}'_z]\mathbf{H}^N + [\mathbf{S}''_z]\mathbf{H}^N$$
$$= \{[\mathbf{S}'_z] + [\mathbf{S}''_z]\}\mathbf{H}^N = [\tilde{\mathbf{S}}_z]\mathbf{H}^N, \tag{42}$$

where with regard for (39)

$$[\tilde{\mathbf{S}}_\tau] = [\mathbf{S}'_\tau] + [\mathbf{S}''_\tau]$$
$$= \begin{bmatrix} S''_\tau \sin^2\beta'' & -S''_\tau \sin\beta''\cos\beta'' \\ -S''_\tau \sin\beta''\cos\beta'' & S''_\tau + S''_\tau \cos^2\beta'' \end{bmatrix} \tag{43}$$

and

$$[\tilde{\mathbf{S}}_z] = [\mathbf{S}'_z] + [\mathbf{S}''_z] = \begin{bmatrix} -S''_z \sin\beta'' S'_z + S''_z \cos\beta'' \end{bmatrix}. \tag{44}$$

Equating the matrices $[\tilde{\mathbf{S}}_\tau]$ and $[\tilde{\mathbf{S}}_z]$ to the initial matrices $[\mathbf{S}_\tau]$ and $[\mathbf{S}_z]$, we obtain equations ensuring decomposition of the Schmucker horizontal tensor and the Schmucker tipper.

We begin with decomposition of the Schmucker horizontal tensor $[\mathbf{S}_\tau]$. In this problem,

$$\begin{bmatrix} S_{xx} & S_{xy} \\ S_{yx} & S_{yy} \end{bmatrix} = \begin{bmatrix} S''_\tau \sin^2\beta'' & -S''_\tau \sin\beta''\cos\beta'' \\ -S''_\tau \sin\beta''\cos\beta'' & S'_\tau + S''_\tau \cos^2\beta'' \end{bmatrix}, \tag{45}$$

whence we obtain the overdetermined system of four incompatible equations in two unknowns S'_τ and S''_τ:

$$\begin{aligned} S''_\tau \sin^2\beta'' &= S_{xx}, \\ S''_\tau \sin\beta''\cos\beta'' &= -S_{xy}, \\ S''_\tau \sin\beta''\cos\beta'' &= -S_{yx}, \\ S'_\tau + S''_\tau \cos^2\beta'' &= S_{yy}. \end{aligned} \tag{46}$$

We reduce this system with the method of least squares to a system of two normal equations. We have in the matrix form

$$\begin{bmatrix} 1 & k \\ k & 1 \end{bmatrix} \begin{bmatrix} S'_\tau \\ S''_\tau \end{bmatrix} = \begin{bmatrix} A \\ B \end{bmatrix}, \tag{47}$$

where

$$k = \cos^2\beta'' \quad A = S_{yy}$$
$$B = S_{xx}\sin^2\beta'' - (S_{xy} + S_{yx})\sin\beta''\cos\beta'' + S_{yy}\cos^2\beta''.$$

Solving the normal equations, we obtain

$$S'_\tau = \frac{-A + Bk}{k^2 - 1}, \quad S''_\tau = \frac{Ak - B}{k^2 - 1}. \tag{48}$$

Substitution of (48) into (40) yields the partial matrices $[S'_\tau]$ and $[S''_\tau]$, the sum of which approaches the initial matrix $[\mathbf{S}_\tau]$:

$$[S'_\tau] = \frac{-A+Bk}{k^2-1}\begin{bmatrix}0 & 0\\ 0 & 1\end{bmatrix},$$
$$[S''_\tau] = \frac{Ak-B}{k^2-1}\begin{bmatrix}\sin^2\beta'' & -\sin\beta''\cos\beta''\\ -\sin\beta''\cos\beta'' & \cos^2\beta''\end{bmatrix}. \quad (49)$$

We now turn to the decomposition of the Schmucker tipper $[\mathbf{S}_z]$. In this problem,

$$\begin{bmatrix}S_{zx} & S_{zy}\end{bmatrix} = \begin{bmatrix}-S''_z\sin\beta'' & S'_z + S''_z\cos\beta''\end{bmatrix}, \quad (50)$$

whence we obtain a system of two linear equations in two unknowns S'_z and S''_z:

$$S''_z\sin\beta'' = -S_{zx},$$
$$S'_z + S''_z\cos\beta'' = S_{zy}. \quad (51)$$

Solving these equations, we have

$$S'_z = S_{zx}\cot\beta'' + S_{zy}, \quad S''_z = -S_{zx}/\sin\beta''. \quad (52)$$

Substitution of (52) into (40) yields the partial matrices

$$[\mathbf{S}'_z] = \begin{bmatrix}0 & S_{zx}\cot\beta'' + S_{zy}\end{bmatrix},$$
$$[\mathbf{S}''_z] = \begin{bmatrix}S_{zx} & -S_{zx}\cot\beta''\end{bmatrix}, \quad (53)$$

whose sum $[\tilde{\mathbf{S}}_z]$ is equal to the initial matrix $[\mathbf{S}_z]$.

Let us return to the model $\{P_1P_2\}$ shown in Fig. 5. Let the initial matrices $[\mathbf{S}_\tau]$ and $[\mathbf{S}_z]$ be given in this model. The decomposition of matrices $[\mathbf{S}_\tau]$ and $[\mathbf{S}_z]$ into the partial matrices $[\mathbf{S}'_\tau]$, $[\mathbf{S}''_\tau]$ and $[\mathbf{S}'_z]$, $[\mathbf{S}''_z]$ is shown in Figs. 8 and 9. Here, in the range of periods $T = 100$–10000 s, the pseudotopographies of the matrices $[\mathbf{S}'_\tau]$, $[\mathbf{S}''_\tau]]$ and $[\mathbf{S}'_z]$, $[\mathbf{S}''_z]$, obtained in the model $\{P_1P_2\}$ with (49) and (53) are close to the pseudotopographies of the matrices $[\bar{\mathbf{S}}'_\tau]$, $[\bar{\mathbf{S}}''_\tau]$ and $[\bar{\mathbf{S}}'_z]$, $[\bar{\mathbf{S}}''_z]$ obtained in the models $\{P_1\}$ and $\{P_2\}$ by direct calculations. This evidences a sufficient accuracy of the decomposition. We conclude that the pseudotopography of the norm of each of the partial matrices $[\mathbf{S}'_\tau]$, $[\mathbf{S}''_\tau]$ and $[\mathbf{S}'_z]$, $[\mathbf{S}''_z]$ reflects the dominating effect of the corresponding anomaly-forming structure. Thus, the inversion of the 3D matrices $[\mathbf{S}_\tau]$ and $[\mathbf{S}_z]$ may be reduced to independent inversions of the 2D matrices $[\mathbf{S}'_\tau]$, $[\mathbf{S}''_\tau]$ and $[\mathbf{S}'_z]$, $[\mathbf{S}''_z]$.

An analogous result may be obtained directly with the Schmucker induction arrows $\mathrm{Re}\mathbf{S}_z$ and $\mathrm{Im}\mathbf{S}_z$, which allow one to determine the strike of the anomaly-forming structures P_1 and P_2 in favorable frequency intervals. If $\beta'' = \alpha'' - \alpha'$ is given, the initial real and imaginary induction arrows $\mathrm{Re}\mathbf{S}_z$ and $\mathrm{Im}\mathbf{S}_z$ decompose into the sum of the partial induction arrows $\mathrm{Re}\mathbf{S}'_z$, $\mathrm{Im}\mathbf{S}'_z$ and $\mathrm{Re}\mathbf{S}''_z$, $\mathrm{Im}\mathbf{S}''_z$, directed along the y and y'' axes, i.e., perpendicularly to the strike of the structures P_1 and P_2. According to (51) and (52),

$$\mathrm{Re}\mathbf{S}_z = \mathrm{Re}\mathbf{S}'_z + \mathrm{Re}\mathbf{S}''_z,$$
$$\mathrm{Im}\mathbf{S}_z = \mathrm{Im}\mathbf{S}'_z + \mathrm{Im}\mathbf{S}''_z, \quad (54)$$

where

$$\mathrm{Re}\mathbf{S}_z = \mathrm{Re}S_{zx}\mathbf{1}_x + \mathrm{Re}S_{zy}\mathbf{1}_y,$$
$$\mathrm{Im}\mathbf{S}_z = \mathrm{Im}S_{zx}\mathbf{1}_x + \mathrm{Im}S_{zy}\mathbf{1}_y,$$
$$\mathrm{Re}\mathbf{S}'_z = (\mathrm{Re}S_{zx}\cot\beta'' + \mathrm{Re}S_{zy})\mathbf{1}_y = \mathrm{Re}S'_z\mathbf{1}_y,$$
$$\mathrm{Im}\mathbf{S}'_z = (\mathrm{Im}S_{zx}\cot\beta'' + \mathrm{Im}S_{zy})\mathbf{1}_y = \mathrm{Im}S'_z\mathbf{1}_y,$$
$$\mathrm{Re}\mathbf{S}''_z = \mathrm{Re}S_{zx}\mathbf{1}_x - \mathrm{Re}S_{zx}\cot\beta''\mathbf{1}_y = \mathrm{Re}S''_z\mathbf{1}''_y,$$
$$\mathrm{Im}\mathbf{S}''_z = \mathrm{Im}S_{zx}\mathbf{1}_x - \mathrm{Im}S_{zx}\cot\beta''\mathbf{1}_y = \mathrm{Im}S''_z\mathbf{1}''_y.$$

This method may be effective in the case of an irregular observation network hampering the construction of the magnetovariational pseudotopographies.

It is noteworthy that the decomposition of the Schmucker horizontal magnetic tensor in the second problem is reduced to the solution of an overdetermined system of equations, which allows one to incorporate the angles of strike of the structures P_1 and P_2 into the set of unknowns. This complicates the problem solution (the equations become nonlinear), but may increase its efficiency.

The third problem is to separate local and regional magnetovariational effects. The methods of decomposition of the magnetovariational response functions $[\mathbf{S}_\tau]$ and $[\mathbf{S}_z]$ considered in the second problem can be adapted easily to the third problem, whose goal is to separate effects of local and regional structures. Ideas developed in [Zhang et al., 1993; Ritter and Banks, 1998] underlie the third magnetovariational problem.

In order to demonstrate the third problem, we will consider the model proposed by Ledo [2006]. The Ledo model contains a regional 2D high-resistance structure P_R imitating a bulge in the crystalline basement and a local 3D low-resistance structure P_L imitating a graphitization zone (Fig. 10). The local structure P_L extends horizontally for a finite length and admits a quasi-2D approximation. The angles of strike of the structures P_R and P_L are equal, respectively, to $\beta^R = 0$ and $\beta^L = 135°$. In the Ledo-I model, the local structure P_L pierces the basement bulge P_R and penetrates into the sedimentary series, while, in the Ledo-II model, this structure is located in the sedimentary series far from the basement bulge P_R.

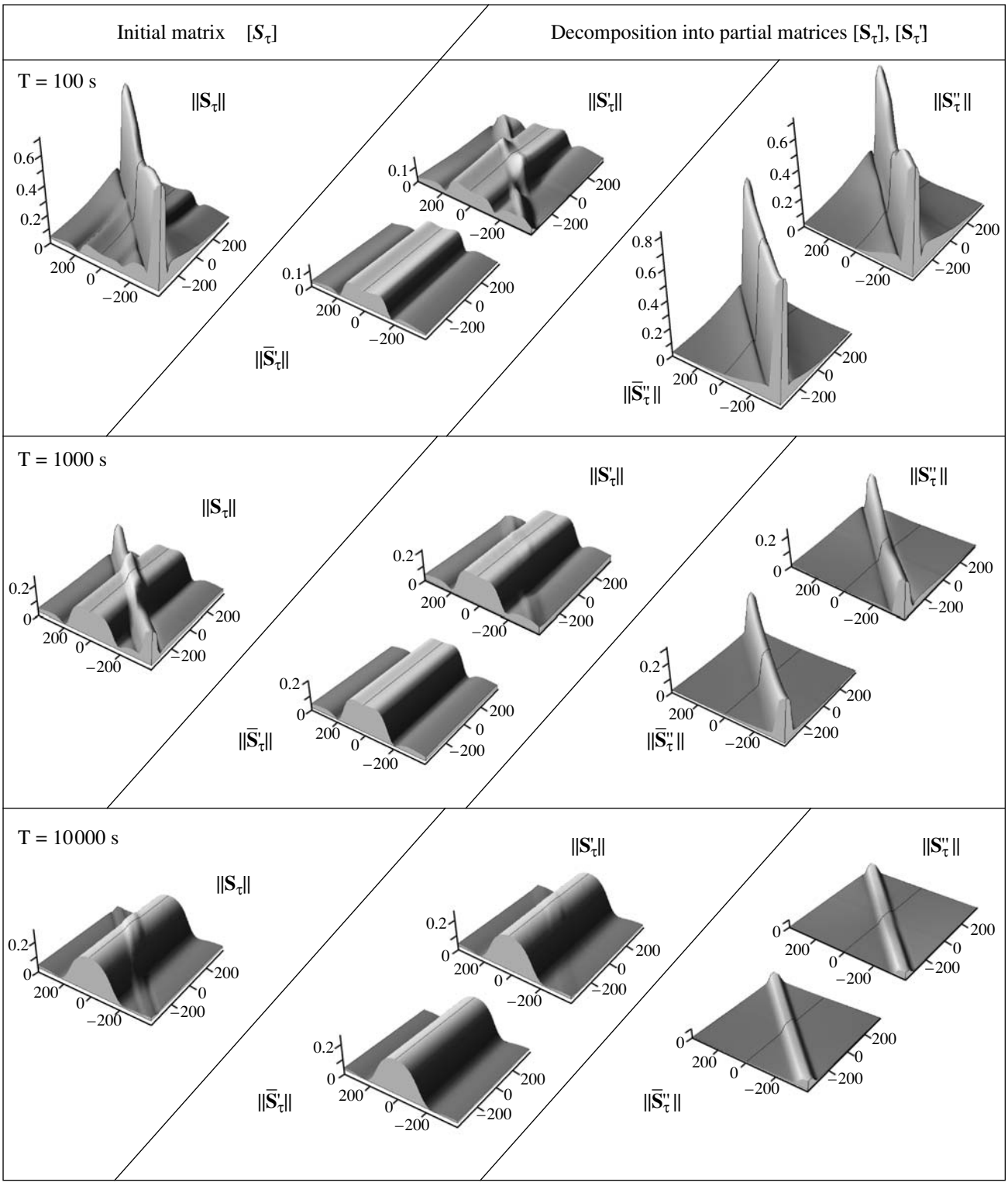

Fig. 8. The decomposition of the initial matrix $[\mathbf{S}_\tau]$ of the Schmucker horizontal magnetic tensor into two partial matrices $[\mathbf{S}'_\tau]$ and $[\mathbf{S}''_\tau]$ in the model $\{P_1P_2\}$ shown in Fig. 5.

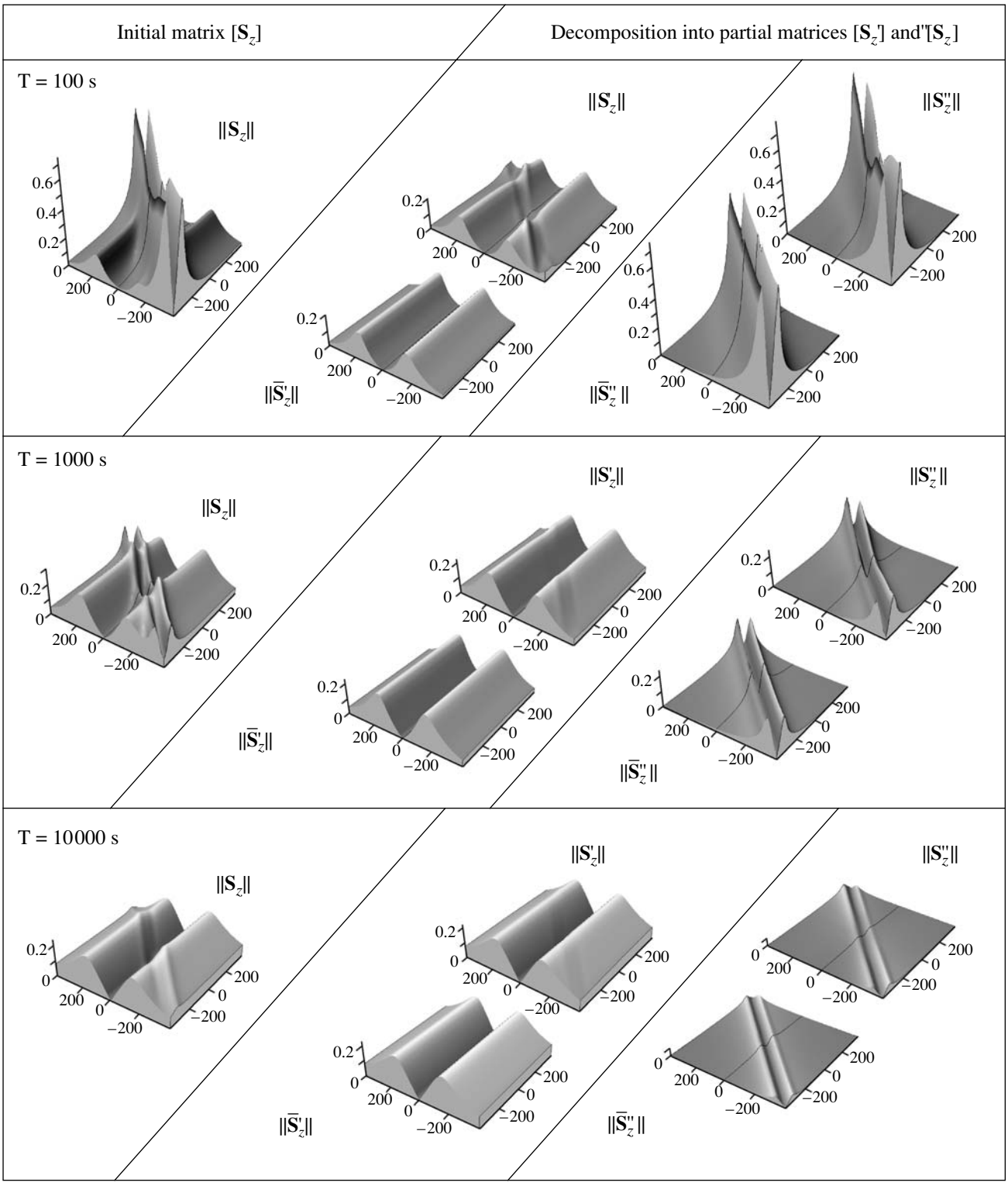

Fig. 9. The decomposition of the initial matrix $[\mathbf{S}_z]$ of the Schmucker tipper into two partial matrices $[\mathbf{S}'_z]$ and $[\mathbf{S}''_z]$ in the model $\{P_1P_2\}$ shown in Fig. 5.

In the case of the Ledo model, the third problem is solved according to the same scheme and in the same succession as the second problem. The angles of strike β^R, β^L are determined using the pseudotopographies of the norms of the Schmucker horizontal magnetic tensor and the Schmucker tipper or using the Schmucker

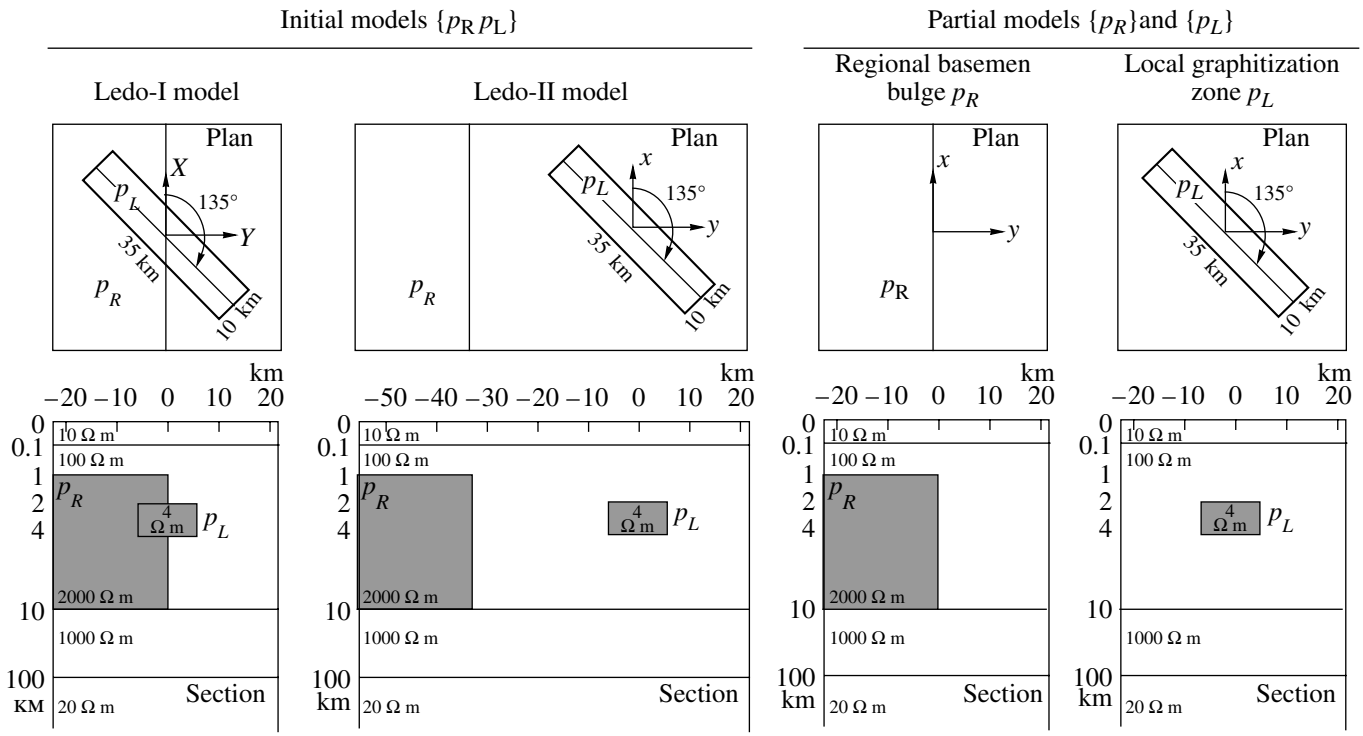

Fig. 10. The Ledo geoelectric models {P_R} and {P_L} and their superposition {$P_R P_L$} include the regional 2D structure P_R and the local horizontally extended 3D structure P_L.

induction arrows. The decomposition of the magnetic tensor and the tipper is performed by formulas (45)–(49) and (50)–(53). Formula (54) is used for the decomposition of the induction arrows. The following change of superscripts is performed in all these formulas: $S'_\tau \longrightarrow S^R_\tau$, $S''_\tau \longrightarrow S^L_\tau$, $S'_z \longrightarrow S^R_z$, $S''_z \longrightarrow S^L_z$, $\beta'' \longrightarrow \beta^L$.

The separation of the local and regional effects in the Ledo-I model is shown in Figs. 11 and 12. Here, the local structure P_L is in contact with the regional structure P_R. It seems evident that, in this case, the structures should interact more or less strongly, violating the principle of independent superposition. The accuracy of decomposition of the magnetovariational response functions should decrease.

Figure 11 illustrates the decomposition of the Schmucker horizontal magnetic tensor $[\mathbf{S}_\tau]$ performed by formulas (46)–(49) for periods $T = 1$, 10, and 100 s. We will compare the pseudotopographies of the norms of the partial matrices $[\mathbf{S}^R_\tau]$ and $[\mathbf{S}^L_\tau]$ obtained by the decomposition of the initial matrix $[\mathbf{S}_\tau]$ with those of the norms of the partial matrices $[\bar{\mathbf{S}}^R_\tau]$ and $[\bar{\mathbf{S}}^L_\tau]$, obtained via direct calculations in the models P_R and P_L. In the entire range of periods, traces of the local structure recognizable on the pseudotopography of the regional matrix $[\mathbf{S}^R_\tau]$ are not found on the pseudotopography of the matrix $[\bar{\mathbf{S}}^R_\tau]$. At the same time, the pseudotopography of the local matrix $[\mathbf{S}^L_\tau]$ virtually duplicates the pseudotopography of the matrix $[\bar{\mathbf{S}}^L_\tau]$. Note that the defects of the matrix $[\mathbf{S}^R_\tau]$ are easily eliminated by smoothing the components of the tensor $[\mathbf{S}^R_\tau]$ on profiles directed along the regional strike.

We now pass to Fig. 12, illustrating the decomposition of the Schmucker tipper performed by formulas (50)–(53) for periods $T = 1$, 10, and 100 s. Let us compare the pseudotopography of the norms of the partial matrices $[\mathbf{S}^R_z]$ and $[\mathbf{S}^L_z]$ obtained through decomposition of the initial matrix $[\mathbf{S}_z]$ with those of the norms of the matrices $[\bar{\mathbf{S}}^R_z]$ and $[\bar{\mathbf{S}}^L_z]$ obtained through direct calculations in the models P_R and P_L. We see that the decomposition accuracy becomes considerably worse. The traces of the local structure distorting the pseudotopography of the regional matrix $[\mathbf{S}^R_z]$ become sharper, while the side closing clearly seen in the pseudotopography of the matrix $[\mathbf{S}^L_z]$ at $T = 1$ s is not found in the pseudotopography of the local matrix $[\bar{\mathbf{S}}^L_z]$.

The separation of the local and regional effects in the Ledo-II model is shown in Figs. 13 and 14. Here, the local structure P_L is far from the regional structure P_R. In this case, the interaction between the local and regional structures weakens and the principle of independent superposition ensures a sufficiently high accu-

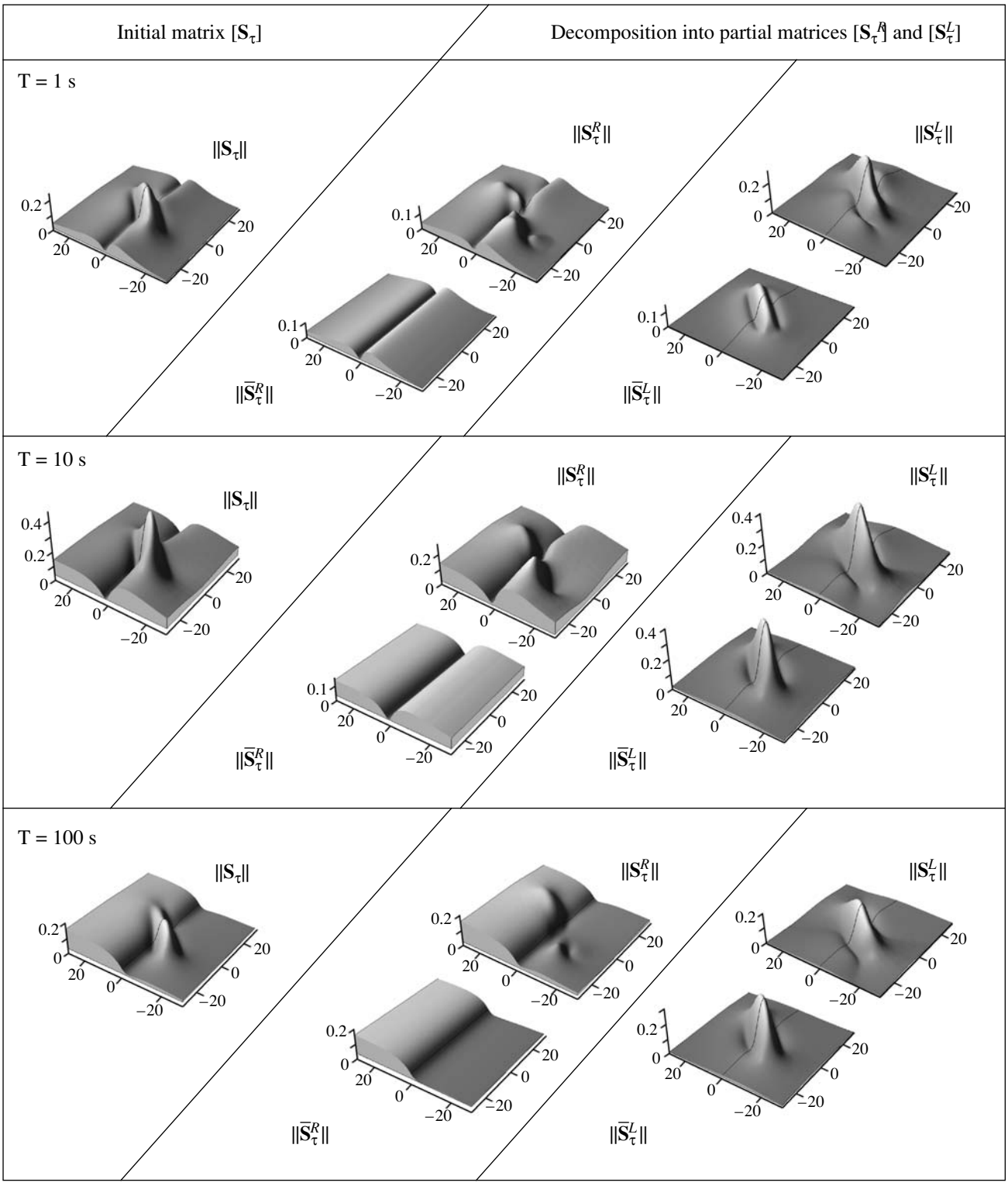

Fig. 11. The decomposition of the initial matrix $[\mathbf{S}_\tau]$ of the Schmucker horizontal magnetic tensor into two partial matrices $[\mathbf{S}_\tau^R]$ and $[\mathbf{S}_\tau^L]$ in the Ledo-I model $\{P_R P_L\}$ shown in Fig. 10.

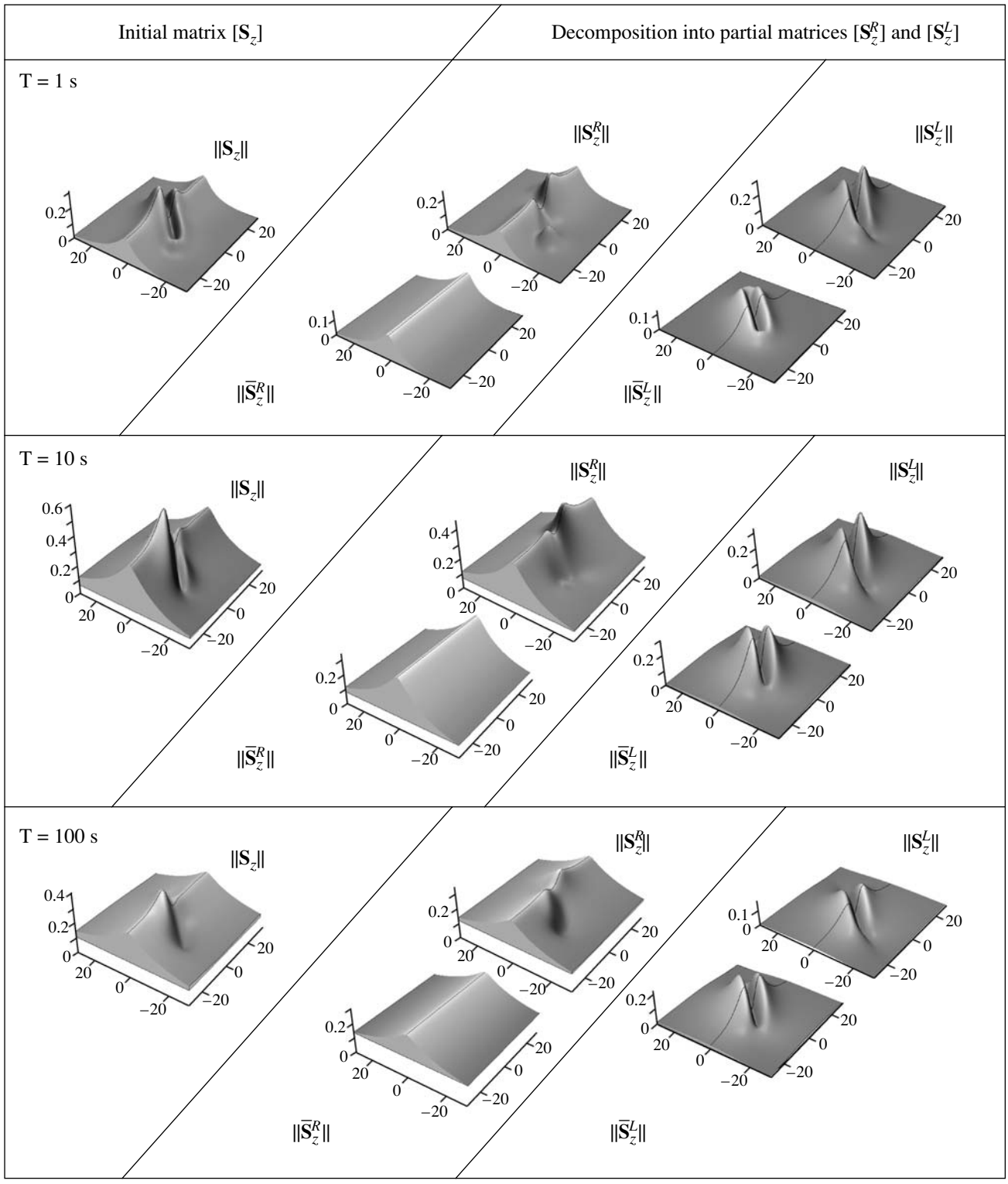

Fig. 12. The decomposition of the initial matrix [$\mathbf{S}_z$] of the Schmucker tipper into two partial matrices [$\mathbf{S}_\tau^R$] and [$\mathbf{S}_\tau^L$] in the Ledo-I model $\{P_R P_L\}$ shown in Fig. 10.

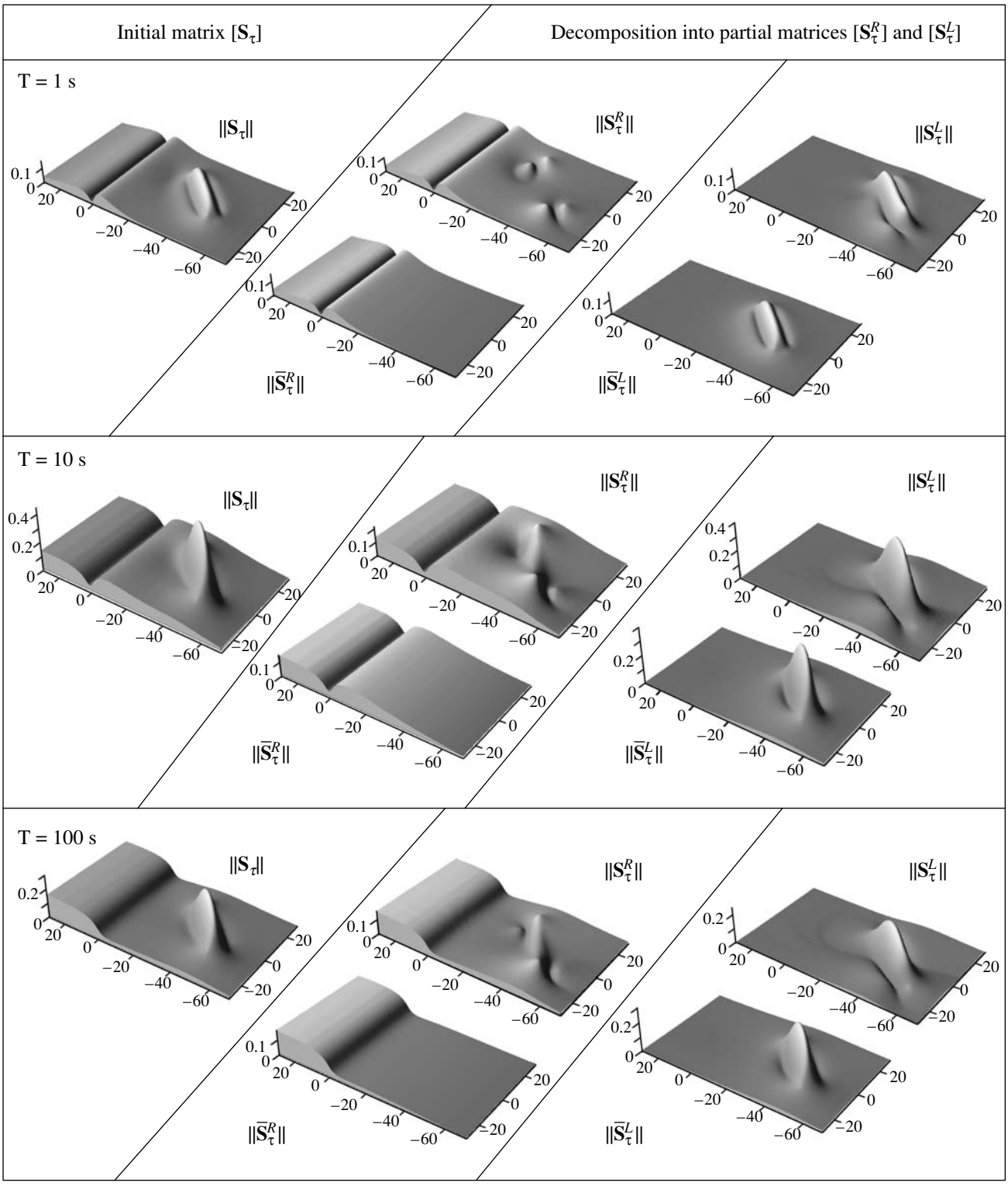

Fig. 13. The decomposition of the initial matrix $[\mathbf{S}_\tau]$ of the Schmucker horizontal magnetic tensor into two partial matrices $[\mathbf{S}_\tau^R]$ and $[\mathbf{S}_\tau^L]$ in the Ledo-II model $\{P_R P_L\}$ shown in Fig. 10.

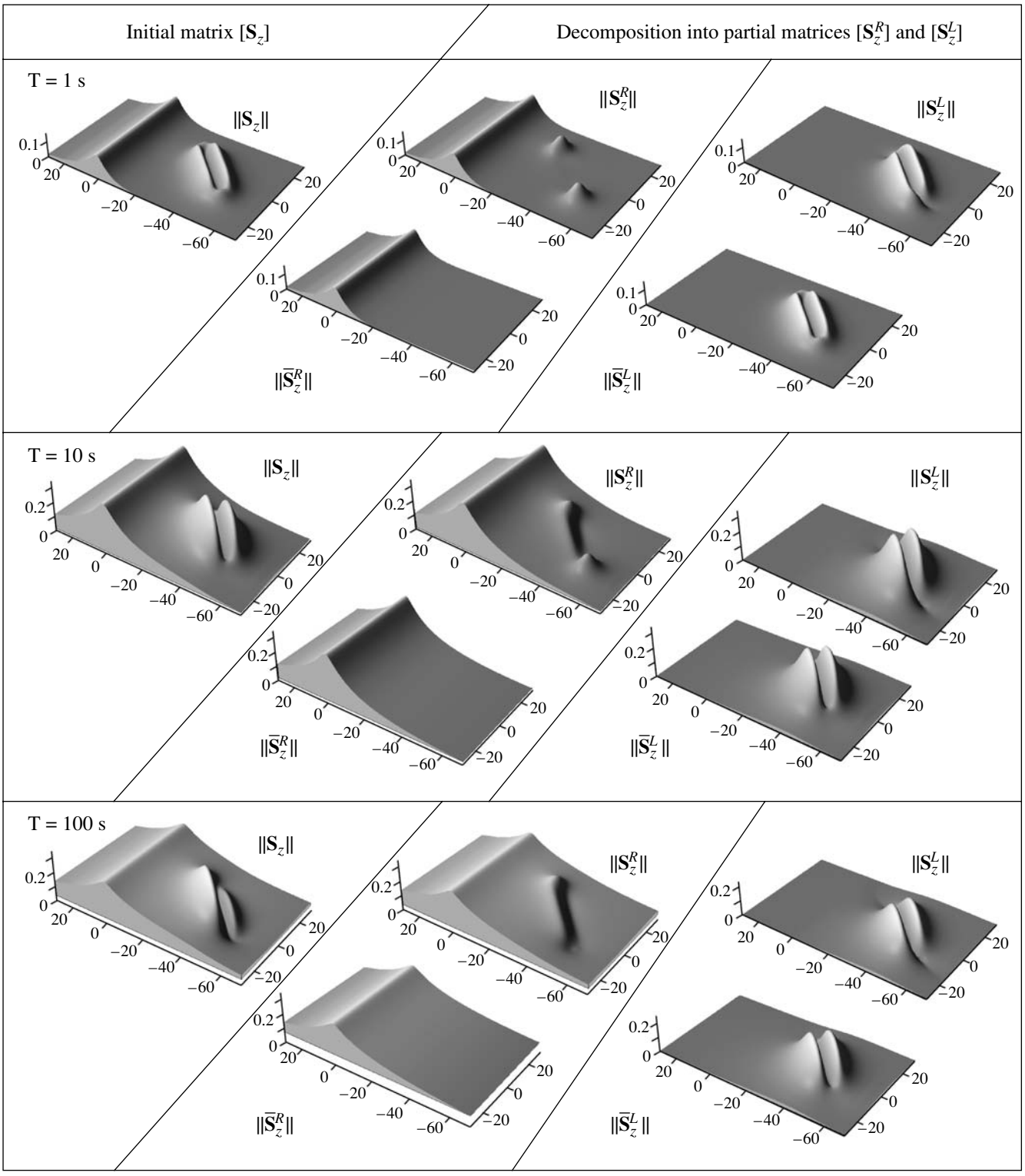

Fig. 14. The decomposition of the initial matrix $[\mathbf{S}_z]$ of the Schmucker tipper into two partial matrices $[\mathbf{S}_\tau^R]$ and $[\mathbf{S}_\tau^L]$ in the Ledo-II model $\{P_R P_L\}$ shown in Fig. 10.

racy of decomposition of the horizontal magnetic tensor [$\mathbf{S}_\tau$] and tipper [$\mathbf{S}_z$].

Generalizing the results of the analysis of the Ledo-I and Ledo-II models, we note that local and regional magnetovariational effects are best separated using the Schmucker magnetic tensor. If the target of magnetovariational sounding is a horizontally extended local structure, decomposition of the horizontal magnetic tensor allows one to eliminate the effects of 2D structures of the regional background.

Note that, in the first, second, and third problems, we may use relations (21) and join the decompositions of the horizontal magnetic tensor [$\mathbf{S}_\tau$] and tipper [$\mathbf{S}_z$] to the decompositions of the horizontal magnetic tensor [**M**] and tipper [**W**].

CONCLUSIONS

From the results obtained in this paper, we conclude that magnetovariational sounding opens new approaches to the interpretation of geoelectric data. This path allows one to increase the sounding resolution, and inversions focused on certain structures become possible.

ACKNOWLEDGMENTS

The author thanks U. Schmucker, a friendly chat with whom inspired the idea of this paper, and D. Yakovlev for preparation of graphic illustrations.

This work was supported by the Russian Foundation for Basic Research, project nos. 07-05-00523 and 08-05-00345.

REFERENCES

1. M. N. Berdichevsky, *Electrical Prospecting by the Method of Magnitovariational Profiling* (Nedra, Moscow, 1968) [in Russian].
2. M. N. Berdichevsky and V. I. Dmitriev, "Magnetotellurics in the Context of the Theory of Ill-posed Problems," in *Investigations in Geophysics* **11** (Tulsa SEG, 2002), 215 p.
3. M. N. Berdichevsky and V. I. Dmitiev, *Models and Methods of Magnetotellurics* (Springer Verlag, 2008)
4. S. Fujivara and H. Toh, "Geomagnetic Transfer Functions in Japan Obtained by First Order Geomagnetic Survey," J. Geomag. Geoelctr. **48**, 1071
5. J. Ledo, "2-D Versus 3-D Magnetotelluric Data Interpretation," Surveys in Geophysics, **27**, 111 (2006)
6. K. Pajunpaa, I. Lahti, and B. Olafsdottir, "Crustal Conductivity Anomalies in Central Sweden and SW Finland," Geophys. J. Int., **150**, 695, (2002)
7. W. D. Parkinson, "Direction of Rapid Geomagnetic Fluctuation," Geophys. J. **2**, 1 (1959)
8. P. Ritter, R. J. Banks "Separation of Local and Regional Information in Distorted GDS Response Functions by Hypothetical Event Analysis," Geophys.J. Int. **135**, 923 (1998)
9. U. Schmucker, *Anomalies of Geomagnetic Variations in the Southwestern United States* (Univ. of California Press, Berkley, 1970)
10. E. Sokolova, M. Berdichevsky, Iv. Varentsov et al. "Advanced Methods for Joint MT/MV Profile Studies of Active Orogens: the Experience from the Central Tien Shan", in *22 Kolloquim EM Tiefenforshung*, (Chech Republic, Decin, 2007), 10 p.
11. W. Soyer and H. Brasse "A Magneto-Variation Study in the Central Andes of N Chile and SW Bolivia," Geophys. Res. Let. **28** (15), 3023 (2001)
12. L. L. Vayan, M. N. Berdichevskii, P. Yu. Pushkarev et al. "*A Geoelectric Model of the Cascadia Subduction Zone*," Fiz. Zemli, [Phys. Solid Earth **38** (10), 816 (2002)]
13. Iv. M. Varentsov "EMTESZ-Pomerania WG. Method of Horizontal Magnetovariational Sounding: Techniques and Application in the EMTESZ-Pomerania Project", in *21 Kolloquim EM Tiefenforshung (Protokoll, ISSN 0946-7467)* (Holle, Germany, 2007), pp. 111–123
14. Iv. M. Varentsov "Arrays of Simultaneous Electromagnetic Sounding: Design, Data Processing and Analysis: Electromagnetic Sounding of the Earth Interior," in *Methods in Geochemistry and Geophysics, 40* (Elsevir, 2007), pp. 263–277
15. H. Wiese "Geomagnetische Tiefentellurik, Teil 2, *Die Streichrichtung der Untergrund-strukturen des Elektrischen Winderstandes, Ersclossen aus Geomagnetischen Variationen*, Geofis. Pura. Appl. **52**, 3 (1962)
16. P. Zhang, L. B. Pedersen, M. Mareshall et al., "Channaling Contribution to Tipper Vectors: a Magnetic Equivalent to Electrical Distortion," Geophys. J. Int. **113**, 693 (1993)